The Pennsylvania State University

The Graduate School

Department of Aerospace Engineering

Control Theory Analysis of a Three-Axis VTOL Flight Director

A Thesis in

Aerospace Engineering

by

Frank R. Niessen

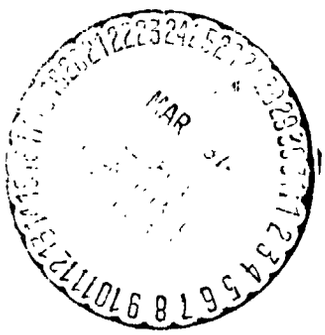

Submitted in Partial Fulfillment
of the Requirements
for the Degree of

Master of Science

June 1971

Date of Approval:

Barnes W. McCormick, Jr.
Head, Department of
Aerospace Engineering
Thesis Adviser

Marshall H. Kaplan
Assistant Professor of
Aerospace Engineering

THESIS - ERRATA SHEET

p. 40 $\frac{1}{\tau_2} = -\frac{Z_w}{m}$

p. 58 $\dot{r}$ eqn $(\psi - \psi')$

p. 59 $\dot{\theta} = q - r\phi$

$\dot{\phi} = p + r\theta$

$\dot{\psi} = r + q\phi$

p. 65 real 0 db line at -21 db, as labeled on figure

p. 67 and 69 "(a)" captions missing

(a) Longitudinal and vertical control axes

p. 73, ref 6 TN D-6108

ACKNOWLEDGMENTS

The author would like to note the valuable assistance of Mr. Steve W. Farmer, Jr., National Aeronautics and Space Administration engineer, who helped to write the computer program for the fixed-base simulation. In addition, the cooperation of both Mr. Robert W. Sommer and Mr. Kenneth R. Yenni, National Aeronautics and Space Administration research test pilots, who participated in the simulator evaluation, is gratefully acknowledged. Also, the author would like to thank Dr. Barnes W. McCormick, Jr., thesis adviser, for offering many helpful suggestions in the final preparation of the thesis.

TABLE OF CONTENTS

LIST OF TABLES

LIST OF ILLUSTRATIONS

Figure Page

SYMBOLS

A, B	polynomial coefficients
D	random disturbance, rad
g	gravitational constant, 32.2 $\frac{ft}{sec}2$
I_x	rolling moment of inertia, slug-ft^2
I_y	pitching moment of inertia, slug-ft^2
I_z	yawing moment of inertia, slug-ft^2
K	gain
L	rolling moment, ft-lb
$\frac{L_p}{I_x}$	roll rate damping derivative, sec^{-1}
$\frac{L_{\delta_a}}{I_x}$	roll control sensitivity, $\frac{rad/sec^2}{in}$
$\frac{L_\phi}{I_x}$	roll attitude damping derivative, sec^{-2}
m	mass, slugs
M	pitching moment, ft-lb
$\frac{M_q}{I_y}$	pitch rate damping derivative, sec^{-1}
$\frac{M_{\delta_e}}{I_y}$	pitch control sensitivity, $\frac{rad/sec^2}{in}$
$\frac{M_\theta}{I_y}$	pitch attitude damping derivative, sec^{-2}
N	yawing moment, ft-lb
$\frac{N_r}{I_z}$	yaw rate damping derivative, sec^{-1}
$\frac{N_v}{I_z}$	yaw due to sideslip derivative, $\frac{rad/sec^2}{ft/sec}$

$\frac{N_{\delta_a}}{I_z}$	yaw due to lateral stick derivative, $\frac{rad/sec^2}{in}$
$\frac{N_{\delta_r}}{I_z}$	yaw control sensitivity, $\frac{rad/sec^2}{in}$
$\frac{N_{\psi}}{I_z}$	yaw attitude damping derivative, sec^{-2}
P	pilot transfer function
p	roll rate, $\frac{rad}{sec}$
q	pitch rate, $\frac{rad}{sec}$
r	yaw rate, $\frac{rad}{sec}$
$s = \sigma + j\omega$	Laplacian operator
t	time, sec
T_s	settling time, sec
u	body-axis longitudinal velocity, $\frac{ft}{sec}$
v	body-axis lateral velocity, $\frac{ft}{sec}$
w	body-axis vertical velocity, $\frac{ft}{sec}$
x, y, z	body-axis coordinates
X, Y, Z	inertial coordinates
$\frac{X_u}{m}$	longitudinal speed stability derivative, sec^{-1}
$\frac{Y_v}{m}$	sideforce due to sideslip derivative, sec^{-1}
$\frac{Z_w}{m}$	vertical velocity damping derivative, sec^{-1}
$\frac{Z_{\delta_p}}{m}$	power control sensitivity, $\frac{ft/sec^2}{in}$

δ	pilot control displacement, in
ϵ	error, rad
ζ	damping ratio
θ	pitch attitude, rad
τ	time constant, sec
ϕ	roll attitude, rad
ψ	yaw attitude, rad
ω	frequency, $\frac{\text{rad}}{\text{sec}}$
ω_n	natural frequency, $\frac{\text{rad}}{\text{sec}}$

Subscripts

a	lateral stick (aileron)
c	commanded value
e	longitudinal stick (elevator)
g	gust
I	pilot lag
L	pilot lead
P	pilot
p	power-control
p_o	power-control trim
r	pedal (rudder)
ϵ	error

CHAPTER I

INTRODUCTION

While vertical take-off and landing (VTOL) aircraft have the obvious advantange of being able to operate from restricted areas, this capability exists only under good visibility conditions. Instrument operation of these aircraft has been precluded because of basic vehicle handling qualities deficiencies and inadequate displays. In reference 12, which discusses VTOL instrument flight research at Langley Research Center, it has been concluded that, along with stability and control augmentation, flight-director display information will be required for routine VTOL instrument operation. However, to be acceptable to the pilot and to be as effective as possible, the flight-director control laws must be tailored both to the pilot and to the specific vehicle dynamics. This implies that conventional flight directors, designed for fixed-wing aircraft, will, in general, not be suitable for low-speed VTOL instrument flight. In the past, flight-director design has been accomplished primarily through trial-and-error adjustment of the flight-director signals either under actual flight conditions or in simulators. Such a design approach can take a considerable amount of time, and therefore, be quite costly, while the resulting flight director is optimum only in a crude sense. Therefore, it would be highly desirable to utilize a more effective design procedure based on a thorough analytical understanding of the overall system closed-loop dynamics.

This thesis will present a control theory analysis of a VTOL flight director and will discuss the results of a fixed-based simulator evaluation of the flight-director commands. The VTOL configuration selected for this study is a helicopter-type VTOL which controls the direction of the thrust vector by means of vehicle-attitude changes and, furthermore, employs high-gain attitude stabilization. This configuration is the same as one which was simulated in actual instrument flight tests with a variable stability helicopter (refs. 6 and 8). Stability analyses are made for each of the flight-director commands, assuming a single input-output, multi-loop system model for each control axis. The analyses proceed from the inner-loops to the outer-loops, using an analytical pilot model selected on the basis of the innermost-loop dynamics. The time response of the analytical model of the system is primarily used to adjust system gains, while root locus plots are used to identify dominant modes and mode interactions. Finally, the fixed-base simulator results are presented, complementing the theoretical analysis.

CHAPTER II

DESCRIPTION OF CONTROL/DISPLAY SYSTEM

The block diagram in figure 1 illustrates the general organization of the control/display system considered in this study. It is assumed that the pilot is actively engaged as a control element in maintaining the guidance and control of the aircraft. As indicated, control augmentation has been provided to stabilize the inner-loop, higher frequency dynamics of the vehicle in an attempt to keep the pilot's workload at an acceptable level.

The VTOL configuration selected for this study employs high-gain stabilization for each of the three angular degrees of freedom. The control augmentation system commands a well damped, second-order attitude response to pilot control inputs in pitch and roll. In yaw, two alternate control modes are provided: the turn following and heading hold modes. In turn following, the aircraft automatically changes heading to eliminate sideslip. Thus, coordinated turns are achieved by simply holding bank angle. Pedal control inputs are used to intentionally produce sideslip if that is desired. In the heading hold mode, the aircraft maintains a given heading in the absence of pedal inputs. Outside of a ± 0.25-inch deadzone, however, a pedal input commands a proportional rate of change of heading. In this mode, lateral maneuvering of the aircraft is accomplished by banking and sideslipping. In the vertical degree of freedom, the basic vehicle has a first-order velocity response to power-control inputs

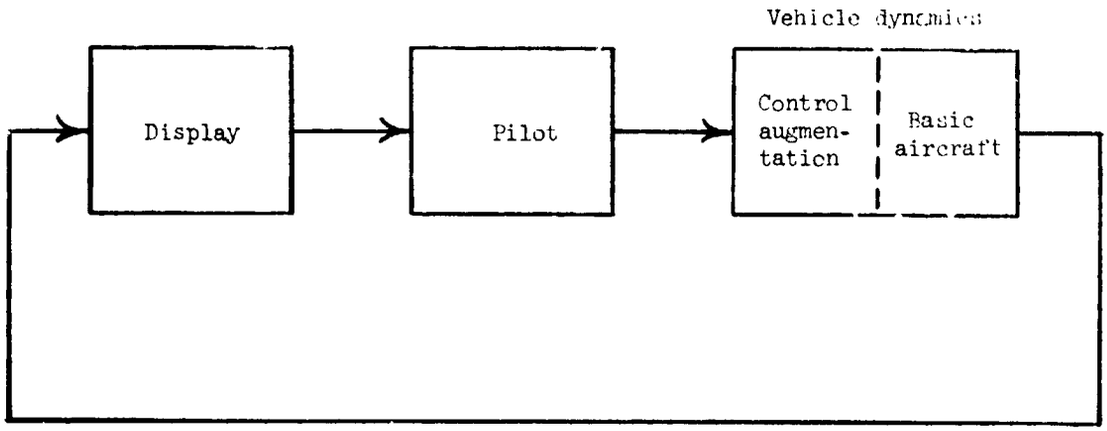

Figure 1.- Control/display system organization.

which was judged to be satisfactory without augmentation. The control response characteristics are listed in table 1. As noted previously, this configuration is the same as that reported in references 6 and 8 which contain more detail on the actual mechanization of the control augmentation system.

It is assumed that the longitudinal speed stability derivative, $X_u/m = -0.025$ sec^{-1}, and sideforce due to sideslip derivative, $Y_v/m = -0.1$ sec^{-1}, of the basic aircraft, are constant over the low speed range considered in this study. The power required curve of the basic aircraft is presented in figure 2 as a plot of power-control position versus airspeed. These data were based on estimates made by the aircraft manufacturer (ref. 3).

The attitude director indicator pictured in figure 3 is the primary display instrument which combines the flight-director commands with a standard attitude indicator. Commands are presented for each of the pilot's control inputs except for pedals, since the control augmentation system controls heading automatically without pedal inputs. Each pilot who participated in the simulator evaluation was allowed to select whichever sensing seemed most natural to him, and most of the pilots preferred the sensing which is indicated in figure 3. For low-speed flight, the aircraft is on the "backside" of the power required curve where an increase in power is required for a decrease in speed. Because of this, altitude is controlled directly with power and speed is controlled with pitch attitude. It is likely that the commands could be displayed in a more effective manner with some other type of director instrument or with an integrated display format, however, the

TABLE 1

CONTROL RESPONSE CHARACTERISTICS

Pitch and Roll	
Attitude sensitivity	$0.15 \frac{\text{rad}}{\text{in}}$
Natural frequency, ω_n	$2.0 \frac{\text{rad}}{\text{sec}}$
Damping ratio, ζ	0.75
Pitch (roll) rate damping, $\frac{M_q}{I_y}\left(\frac{L_p}{I_x}\right)$	$-3.0\ \text{sec}^{-1}$
Pitch (roll) attitude damping, $\frac{M_\theta}{I_y}\left(\frac{L_\phi}{I_x}\right)$	$-4.0\ \text{sec}^{-2}$
Control sensitivity, $\frac{M_{\delta_e}}{I_y}\left(\frac{L_{\delta_a}}{I_x}\right)$	$0.6 \frac{\text{rad/sec}^2}{\text{in}}$
Yaw (heading hold)	
Heading rate sensitivity	$0.35 \frac{\text{rad/sec}}{\text{in}}$
Natural frequency, ω_n	$2.0 \frac{\text{rad}}{\text{sec}}$
Damping ratio, ζ	0.68
Yaw rate damping, $\frac{N_r}{I_z}$	$-2.7\ \text{sec}^{-1}$
Yaw attitude damping, $\frac{N_\psi}{I_z}$	$-4.0\ \text{sec}^{-2}$

TABLE 1.- CONCLUDED

Yaw (turn following)

Control sensitivity, $\frac{N_{\delta_r}}{I_z}$	$0.2 \frac{rad/sec^2}{in}$
Yaw due to sideslip, $\frac{N_v}{I_z}$	$0.004 \frac{rad/sec^2}{ft/sec}$
Yaw rate damping, $\frac{N_r}{I_z}$	$-0.7\ sec^{-1}$
Yaw due to lateral stick, $\frac{N_{\delta_a}}{I_z}$	$0.065 \frac{rad/sec^2}{in}$

Vertical Degree of Freedom

Control sensitivity, $\frac{Z_{\delta_p}}{m}$	$-6.44 \frac{ft/sec^2}{in}$
Vertical velocity damping, $\frac{Z_w}{m}$	$-0.4\ sec^{-1}$

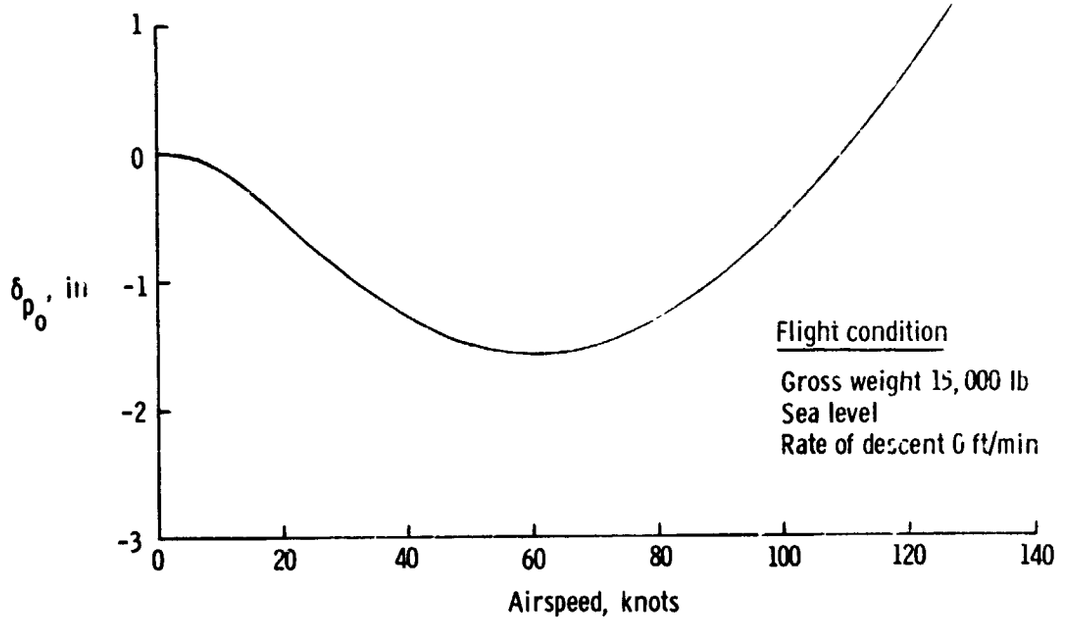

Figure 2.- Power-control trim position vs. airspeed.

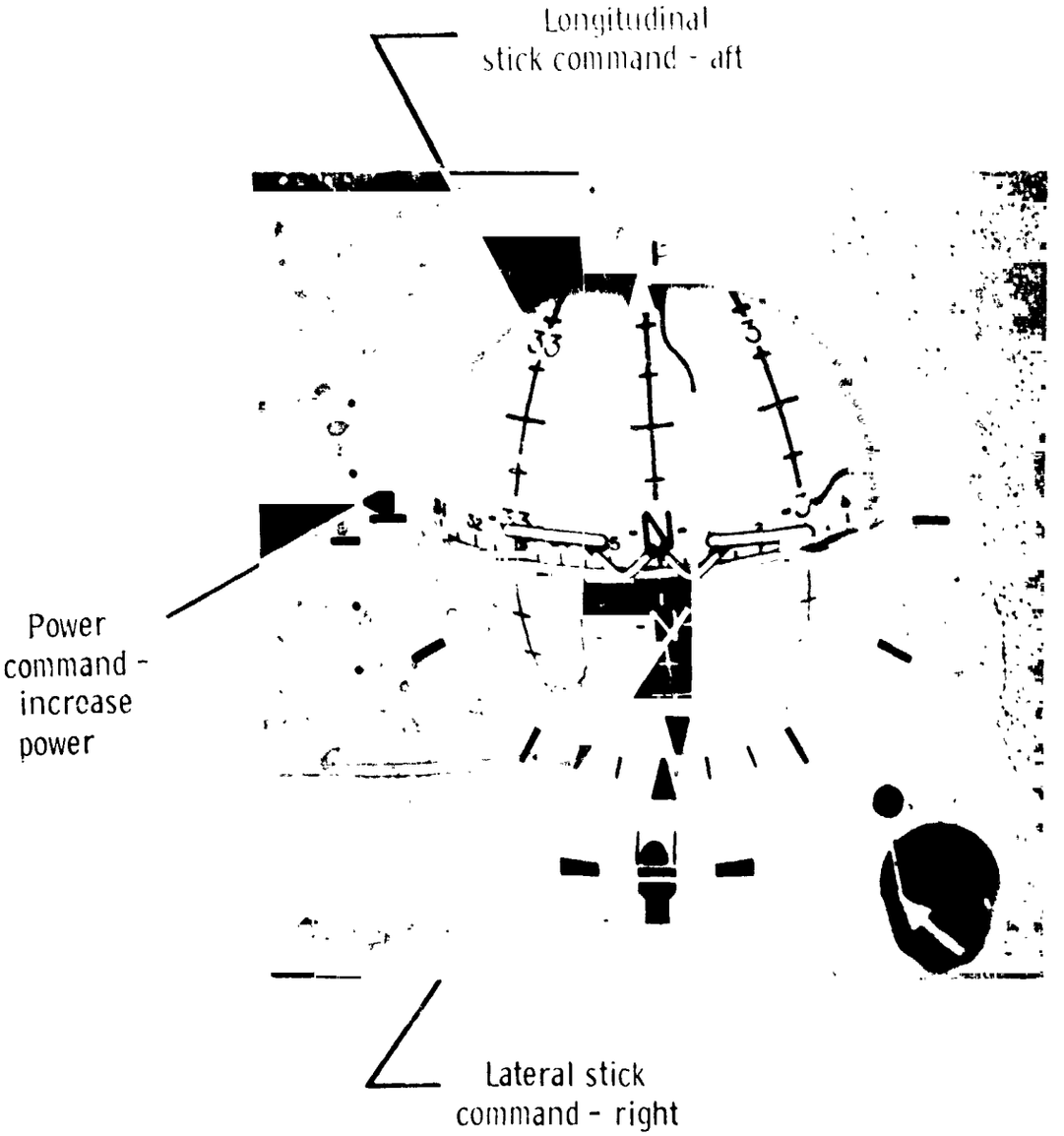

Figure 3.- Attitude director indicator.

present study was limited to the flight-director control laws themselves, not the display hardware. The complete instrument display panel which was used in the simulator is discussed in a later section.

CHAPTER III

THEORETICAL ANALYSIS

The body axes and inertial axes used in the analysis are illustrated in figure 4. The body-fixed axes have the origin at the center of gravity with the x-axis horizontal, and z-axis vertical for steady hovering flight. The inertial or ground-reference axes have the origin at the center of the landing pad, with the X-axis along the runway centerline and the Z-axis positive downward along the vertical.

An actual VTOL landing approach may include many different phases such as level flight prior to acquisition of the runway centerline, descent along the glide slope at constant speed, deceleration, hover, and vertical letdown. Basically, however, the task requires that the aircraft fly according to a set of nominal position or rate profiles which are defined in the inertial coordinate frame. From this general standpoint, the theoretical analysis considers the flight-director control laws on the basis of closed-loop control of ground-referenced position and rate. It is conceivable that navigation equipment such as a precision radar or an inertial platform would be used to provide inertial data in an actual implementation.

The following sections present a detailed stability analysis for each translational degree of freedom as controlled through the corresponding flight-director command. It is assumed that the heading of the aircraft is approximately aligned with the runway centerline so that each case may be studied separately as a single input-output control problem.

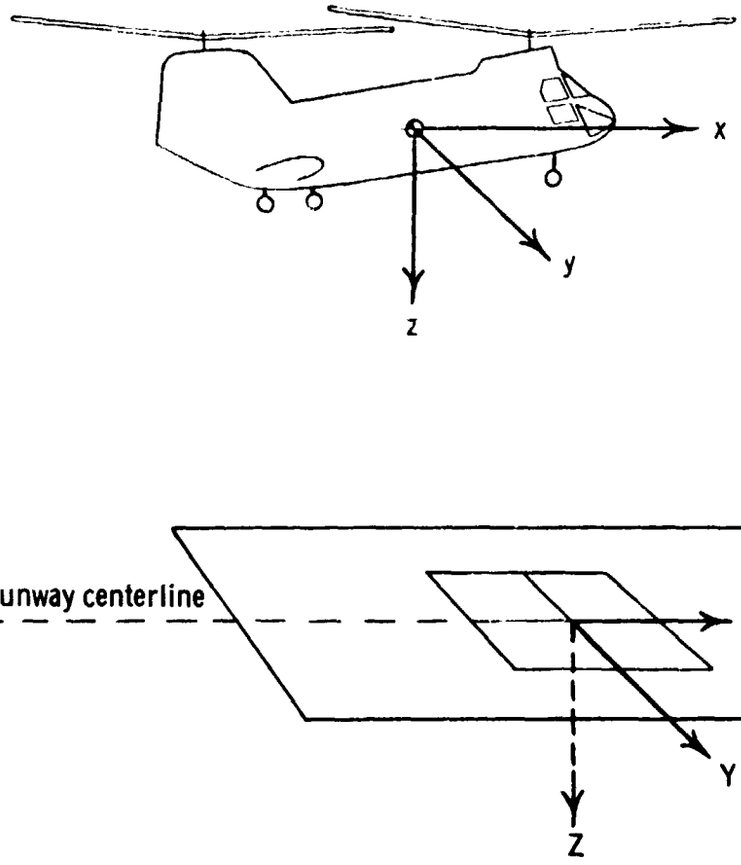

Figure 4.- Body and inertial coordinate frames of reference.

The analytical methods used in the following sections are conventional, classical control theory methods. Laplace transforms are used to indicate input-output dynamics with block diagram rules used to manipulate the various system loops from open- to closed-loop form. Time-response criteria are specified as the basis for adjustment of the flight-director gains, and an analog-computer and an X-Y plotter were employed in generating the time histories. Root locus plots are used in developing further insight by clearly identifying dominant modes and mode interactions. The root locus plots were obtained using a digital computer program. This program computed the coefficients of the characteristic polynomial as functions of the various system parameters and then employed a standard FORTRAN root-solving subroutine to determine the values of the closed-loop roots for each set of specified parameter values.

Longitudinal Control Axis

The basic arrangement of the longitudinal control axis is presented in figure 5. As mentioned previously, the reference steady state flight condition is hover; that is, $\theta = 0$ corresponds to the attitude for hover in the absence of winds. Assuming that aircraft heading is aligned with the runway centerline and that pitch attitude, θ, is a small angle, the transformation from body axes to inertial axes simplifies to $\dot{X} \cong u$. Note that an additional minus sign has been introduced so that for a stable, negative feedback configuration, $K_{\dot{X}}$ is positive. The velocity-control and position-control loops

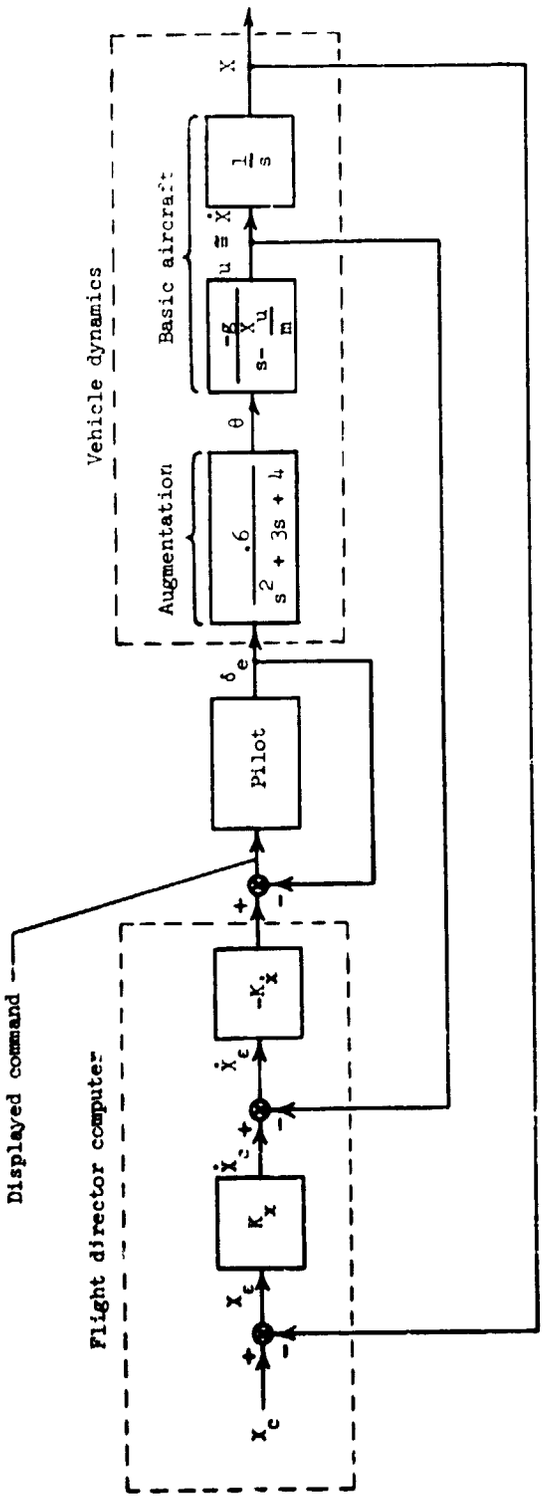

Figure 5.- Basic longitudinal control axis.

and gains are easily identified through this series arrangement of the feedback gains.

It is desirable that the task of centering the flight-director command be as easy as possible, particularly because the pilot has three such commands to follow. For this reason, the flight-director command was made proportional to the difference between the desired stick position and the actual stick position. Thus, when the command bar is centered, the pilot always knows immediately that the aircraft is being flown along the desired approach profile or that the proper input has been made to correct for whatever error may exist. This is consistent with the definition of the "command display" as given in the following quotation.

> The fully augmented or command display does not tell the operator what is happening but instead tells him what to do. The basic information shown on the command display is not the state of something but an ordered action. The command instrument says, in effect, "move your control to this position." The operator need not have any idea of why this action should be taken, but he knows that if he takes it, he will maintain stable control (ref. 7, p. 126).

Since the stick position signal itself is part of the flight-director command, the flight-director controlled-element dynamics would approximate a pure gain for moderate to high frequencies. According to manual control studies (ref. 9), this type of dynamics as compared with rate, $\frac{K}{s}$, and acceleration, $\frac{K}{s^2}$, type dynamics permits the highest cross-over frequency for the pilot/controlled-element open-loop dynamics or, in other words, permits the most rapid closed-loop response with a pilot-in-the-loop.

The analytical model used to represent the response of the pilot in centering the flight-director command was based on results of a previous investigation (ref. 1), in which pilot transfer functions were measured for various single-axis tasks. One of these tasks was to control attitude, θ, subject to a random disturbance, D, and the controlled-element dynamics was a gain of 1.0. This case, shown in figure 6, is identical to the task of centering the flight director signal, assuming that the disturbance input is analogous to the stick position command. Six test pilots and two engineers participated in the study. The measured parameters of the transfer function $\frac{\delta}{D}(s) = \frac{K_p(\tau_L s + 1)}{(\tau_I s + 1)^2}$, as found in reference 1, are listed in table 2. The lead term measured was negligible and the fact that the steady-state gain was slightly less than one was believed to be due to the randomness of the forcing function. If typical values are selected for

$$\frac{\delta}{D}(s) = \frac{1.0}{(0.15s + 1)^2}$$

then the pilot transfer function, P(s), may be determined from

$$\frac{P(s)}{1 + P(s)} = \frac{1.0}{(0.15s + 1)^2}$$

$$P(s) = \frac{3.33}{s(0.075s + 1)}.$$

Thus, the pilot would presumably act as an integrator and a high-frequency, first-order lag in centering the flight-director command.

Using this pilot model, the velocity-control loop is considered first. As drawn in figure 7, the feed-forward path of the longitudinal velocity-control loop lacks a pure integration, and, therefore,

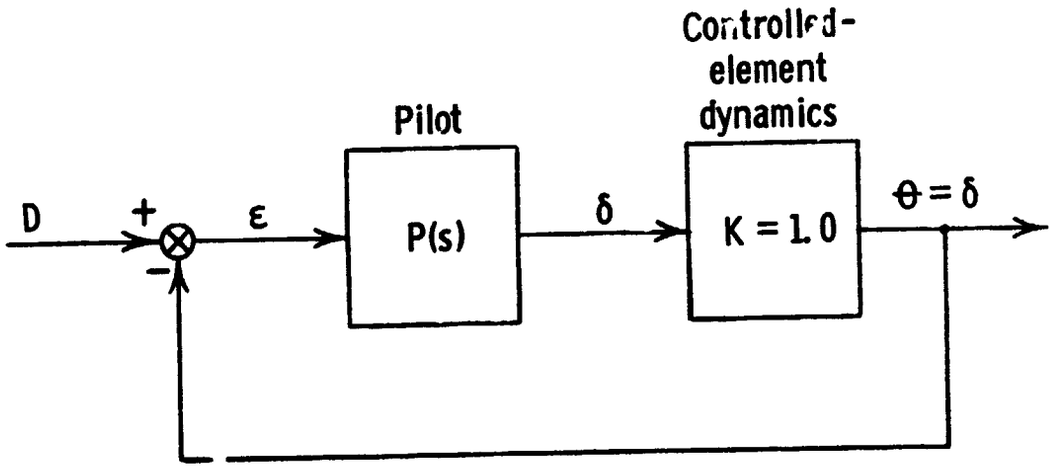

Figure 6.- Single-axis task analogous to task of centering flight director command.

TABLE 2

MEASURED PILOT TRANSFER FUNCTION PARAMETERS
FOR GAIN CONTROLLED-ELEMENT DYNAMICS

Test Subjects	$\frac{\delta}{D}(s) = \frac{K_P(\tau_L s + 1)}{(\tau_I s + 1)^2}$		
	K_P	τ_L	τ_I
Pilot A	1.0	0.0	0.12
Pilot B	0.93	0.0	0.14
Pilot C	0.82	0.0	0.09
Pilot D	0.91	0.09	0.18
Pilot E	0.90	0.0	0.10
Pilot F	0.75	0.25	0.25
Engineer G	0.92	0.08	0.17
Engineer H	1.0	0.33	0.33

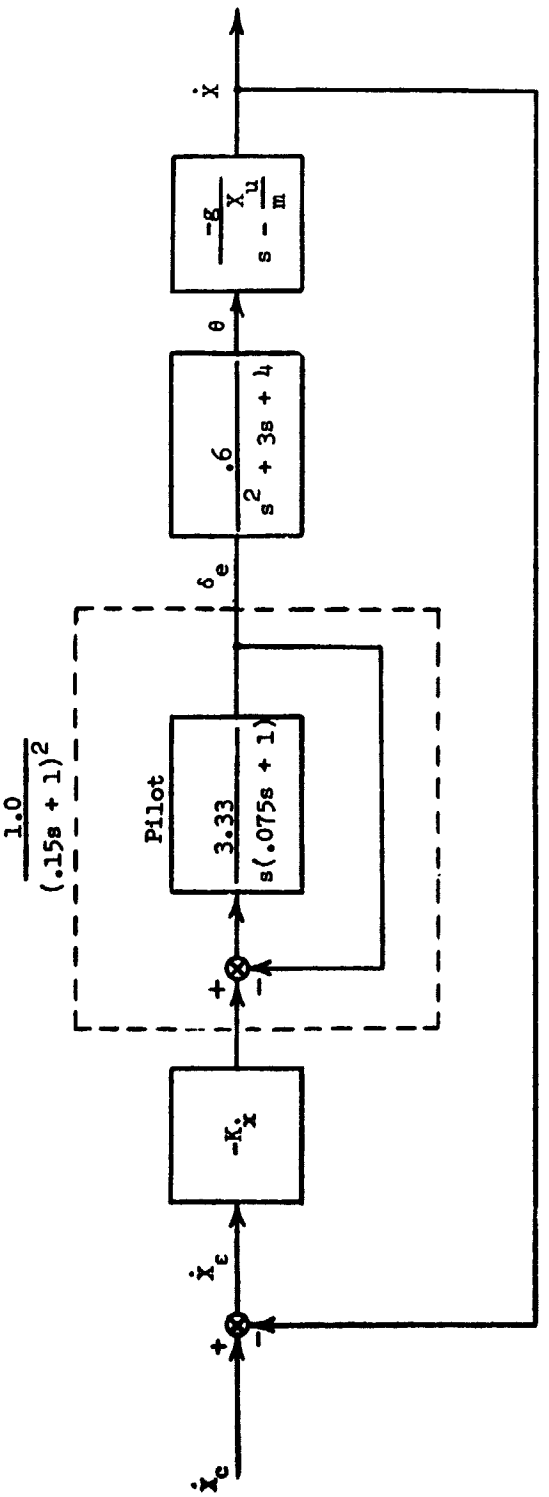

Figure 7.- Longitudinal velocity control with pilot model.

the response to a step, or a constant velocity command, will result in a steady-state error. This may be shown analytically by forming the closed loop transfer function $\frac{\dot{X}}{\dot{X}_c}(s)$ and applying the final-value theorem to $\dot{X}(s)$ for a step input $\dot{X}_c(s) = \frac{1}{s}$.

$$\frac{\dot{X}}{\dot{X}_c}(s) = \frac{K_{\dot{X}}(0.6)(32.2)}{(0.15s + 1)^2(s^2 + 3s + 4)(s + 0.025) + K_{\dot{X}}(0.6)(32.2)}$$

if $\dot{X}_c(s) = \frac{1}{s}$, then $\dot{X}(s) = \frac{1}{s}\frac{\dot{X}}{\dot{X}_c}(s)$

$$\lim_{t \to \infty} \dot{X}(t) = \lim_{s \to 0} \left[s\dot{X}(s)\right] = \frac{193.2\ K_{\dot{X}}}{193.2\ K_{\dot{X}} + 1} < 1.0$$

A practical explanation for the steady-state error is that for a given velocity command, the stick position will generally be some value other than zero and the stick position signal will effectively block part of the velocity error signal. Thus, although the displayed command is zero, a velocity error will exist. For flight directors, this is often referred to as "standoff." It can be seen that the steady-state error will depend on the loop gain, $K_{\dot{X}}$, and, in fact, the error in this case would be quite small, say, on the order of 5 to 10 percent of the commanded velocity for even moderately high gains. However, it is possible to eliminate the error for a step command by effectively adding an integration in the feed-forward path. This can be accomplished by either adding an integration of the velocity error to the commanded stick position, or by washing-out the pilot's stick position

signal on a long-term basis. It will be shown that these two apparently opposite approaches are nearly equivalent from a linear analysis standpoint although they differ somewhat with regard to practical design considerations.

The integrated-error approach, a simple proportional-plus-integral type compensation, introduces an integration along with a zero at $\sigma = -\frac{K_1}{K_{\dot{x}}}$, as shown in figure 8. If an error persists, the integrated error signal gradually increases, demanding an ever larger control displacement until the error is eventually reduced to zero. In the steady-state, the stick position signal is biased by the integrated-error. In practice, however, there are some disadvantages to the integrated-error approach. If the pilot neglects to track the displayed command for some period of time, the integrated-error term could grown extremely large and perhaps result in saturation, even though the actual error remained fairly small. Similarly, large initial errors could also lead to saturation. These problems can be circumvented by simply limiting the integration to values based on estimated maximum stick position or by holding the integration whenever the error is large or the displayed command exceeds some minimum value. The latter technique would ensure that the integrated error would function only when needed to reduce the error to zero and only when the pilot is actually obeying the commands.

The other approach, the stick-washout method, is illustrated in figure 9. On a relatively long-term basis, the stick position signal is washed out by means of a high-pass filter, so that the

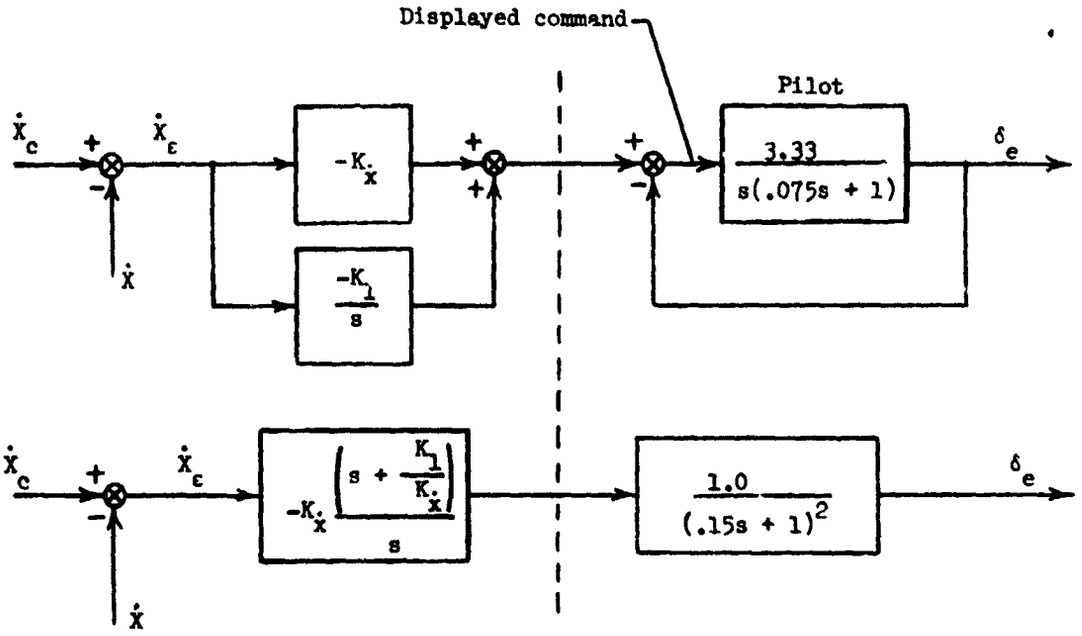

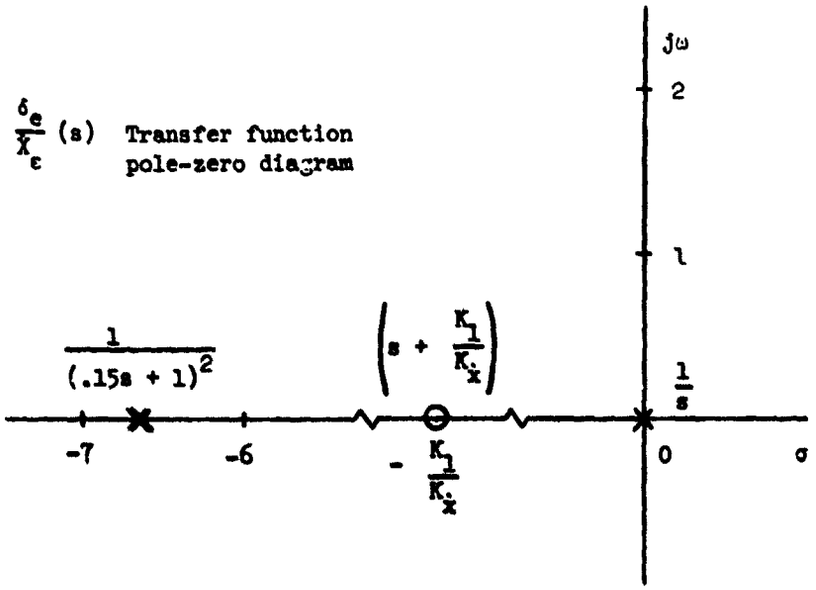

Figure 8.- Integrated-error dynamics.

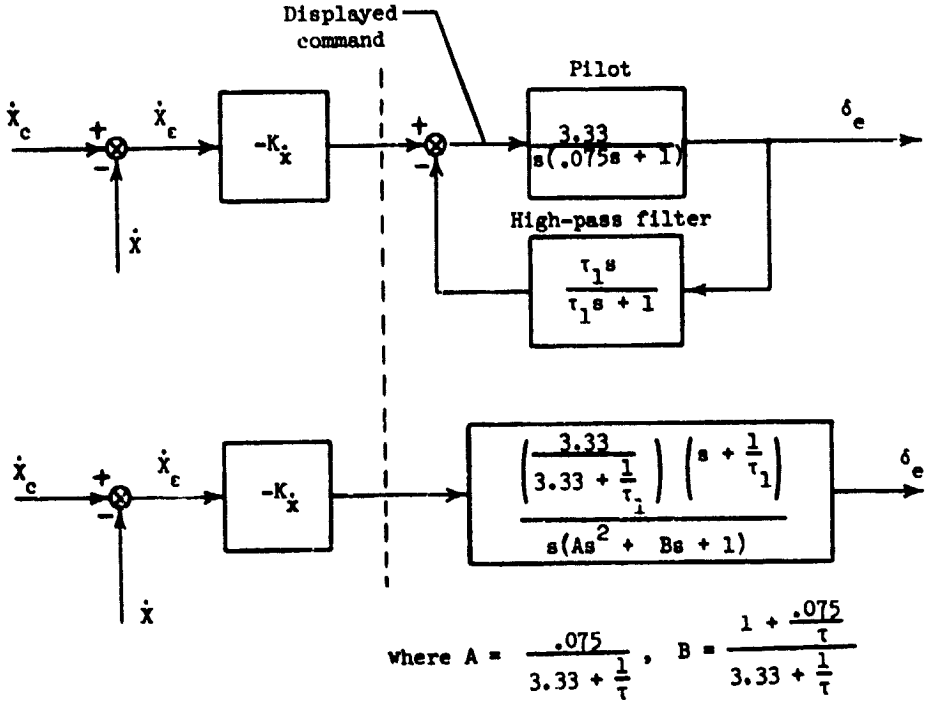

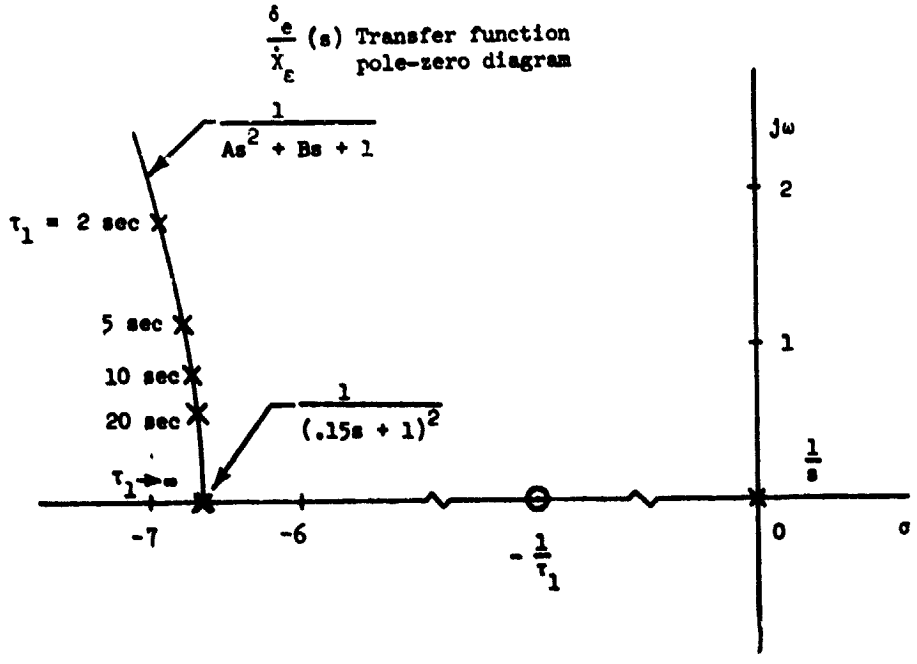

Figure 9.- Stick-washout dynamics.

error signal is never blocked by the steady-state stick position signal. Here, however, there is no free integrator to saturate during periods of pilot inattention. The washout circuit attenuates only very low frequencies and for this reason the pilot model itself is assumed to be unaffected by the stick-washout dynamics. The resulting closed-loop dynamics of the pilot plus stick-washout, as shown in figure 9, contain a pure integration, a zero at $\sigma = -\frac{1}{\tau_1}$, and a pair of complex poles which approximate the double pole $\frac{1.0}{(0.15s + 1)^2}$. For large τ_1, the complex poles merge to the double pole $\frac{1.0}{(0.15s + 1)^2}$ and the static gain approaches 1.0. Comparison of the pole-zero diagrams in figures 8 and 9, which represent the transfer function $\frac{\delta_e}{\dot{X}_\epsilon}(s)$ indicates that if $\frac{K_1}{K_{\dot{X}}^*} = \frac{1}{\tau_1}$, the two approaches are nearly identical from a linear analysis standpoint. Because of its simpler implementation, the washout method is usually considered the more attractive method and will be used here for the rest of the analysis.

For the longitudinal velocity control loop now configured as drawn in figure 10, selection of values for τ_1 and $K_{\dot{X}}^*$ was based on the velocity time-response to a step velocity command. The time-response criterion used was actually determined as a result of the simulator evaluation which was run concurrently with the theoretical analysis. This criterion was that the velocity response for a step input should be well damped, with no more than 1 or 2 percent overshoot, and should reach 95 percent of the commanded velocity within 5 to 6 seconds. The factors involved in the selection of this criterion are discussed in a later section. It was found that the washout time constant, τ_1, the inner-loop parameter, had a significant

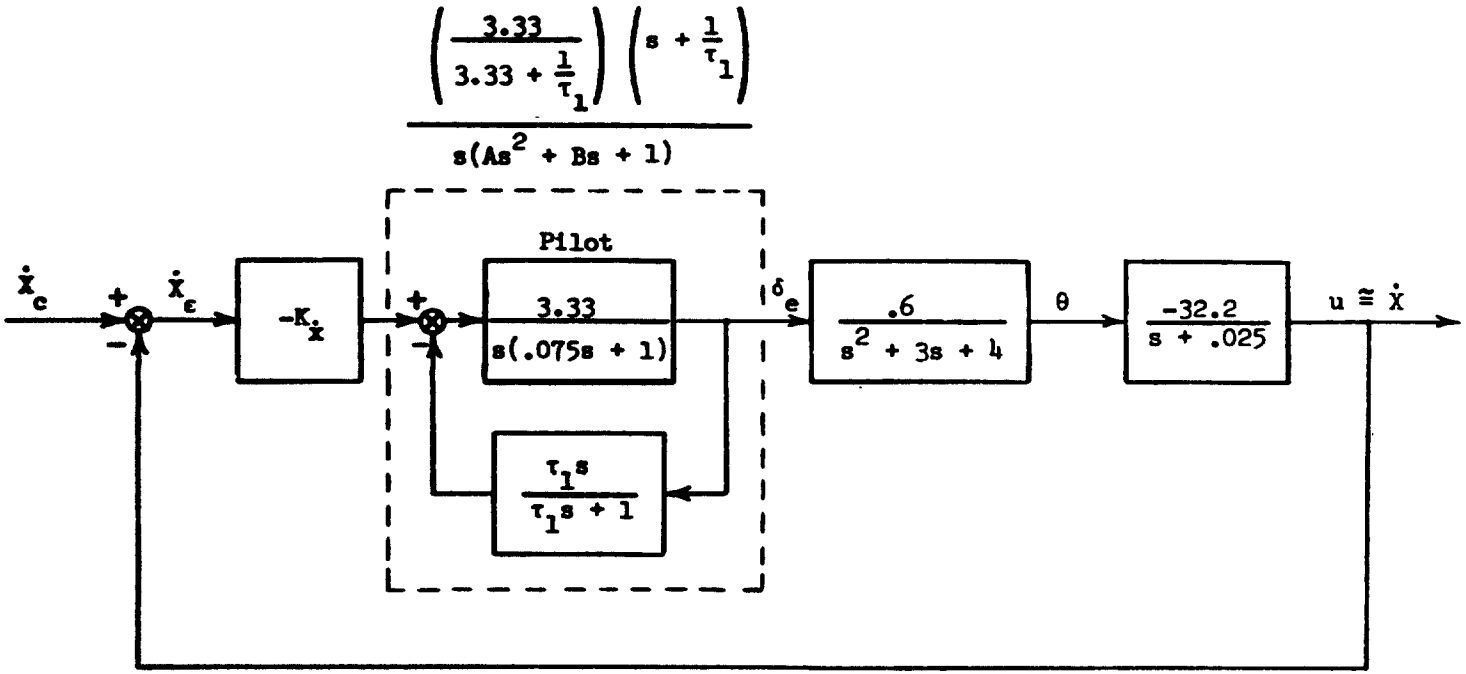

Figure 10.- Longitudinal velocity control with pilot model and stick-washout.

effect on the time response. The time histories in figure 11 show that for low values of τ_1 on the order of 5 seconds, the response is quite underdamped, while for larger values on the order of 10 to 20 seconds, the response is well damped although there is an overshoot which persists for a considerable period of time.

The series of root locus plots in figures 12, 13, and 14, indicate the importance of the location of the zero at $\sigma = -\frac{1}{\tau_1}$ on the closed-loop roots. For $\tau_1 = 5$ sec, the two poles on the real axis at the origin break away and immediately head into the right-half plane. Here, the dominant roots are the complex pair which lie along these branches of the locus resulting in an underdamped response. For $\tau_1 = 20$ sec, these same poles now break away but go around the zero at $\sigma = -\frac{1}{\tau_1}$, and break back onto the real axis. The dominant roots are again a complex pair, however, these lie further in the left-half plane and have a higher damping ratio, yielding a better damped response. The overshoot for $\tau_1 = 20$ sec, as evidenced in the time history, appears to be due to the closed-loop root near the zero at $\sigma = -\frac{1}{\tau_1}$. This low-frequency, first-order pole is apparently not near enough to the zero to have its effect completely cancelled. Selection of $\frac{1}{\tau_1} = \left(\frac{-X_u}{m}\right)$, or $\tau_1 = 40$ sec, however, ensures that the low-frequency mode associated with the drag-damping characteristic of the aircraft will be exactly cancelled and at the same time will reduce the order of the response. The physical significance of selecting $\frac{1}{\tau_1} = \left(\frac{-X_u}{m}\right)$ is that the pilot's stick position signal is thereby washed out at the same rate as the longitudinal velocity response reaches steady state due to the drag-damping of the aircraft.

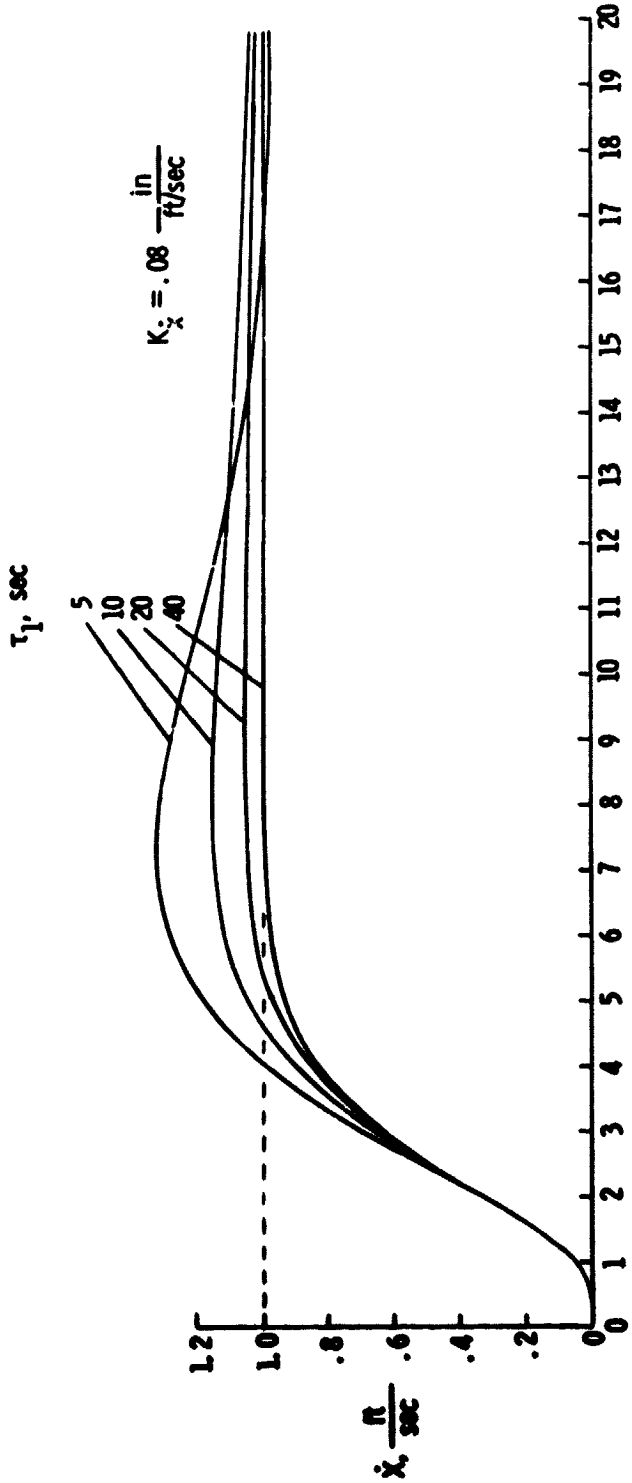

Figure 11.- Longitudinal velocity time response to step command for various τ_1.

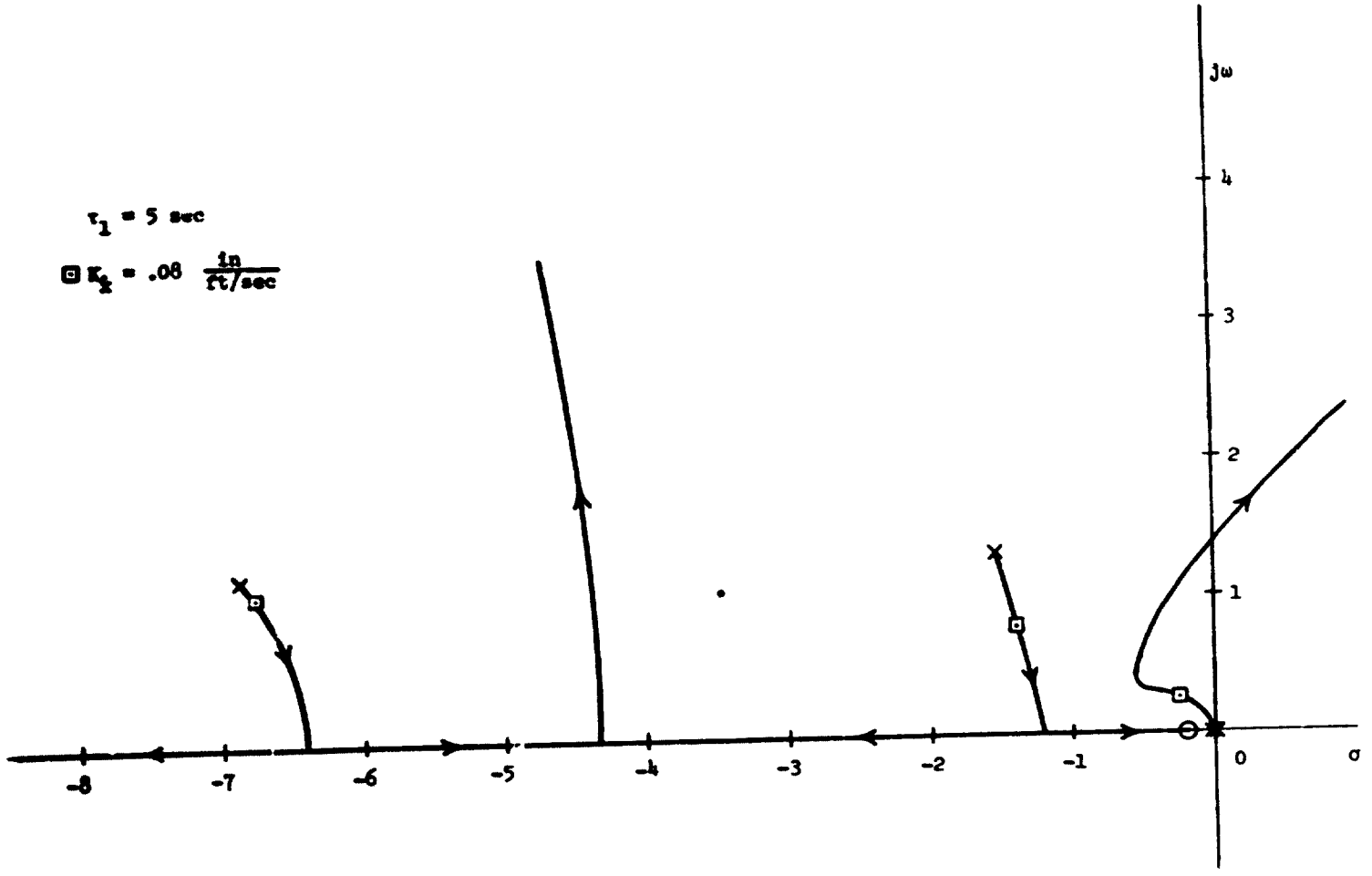

Figure 12.- Root locus for longitudinal velocity control, τ_1 = 5 sec.

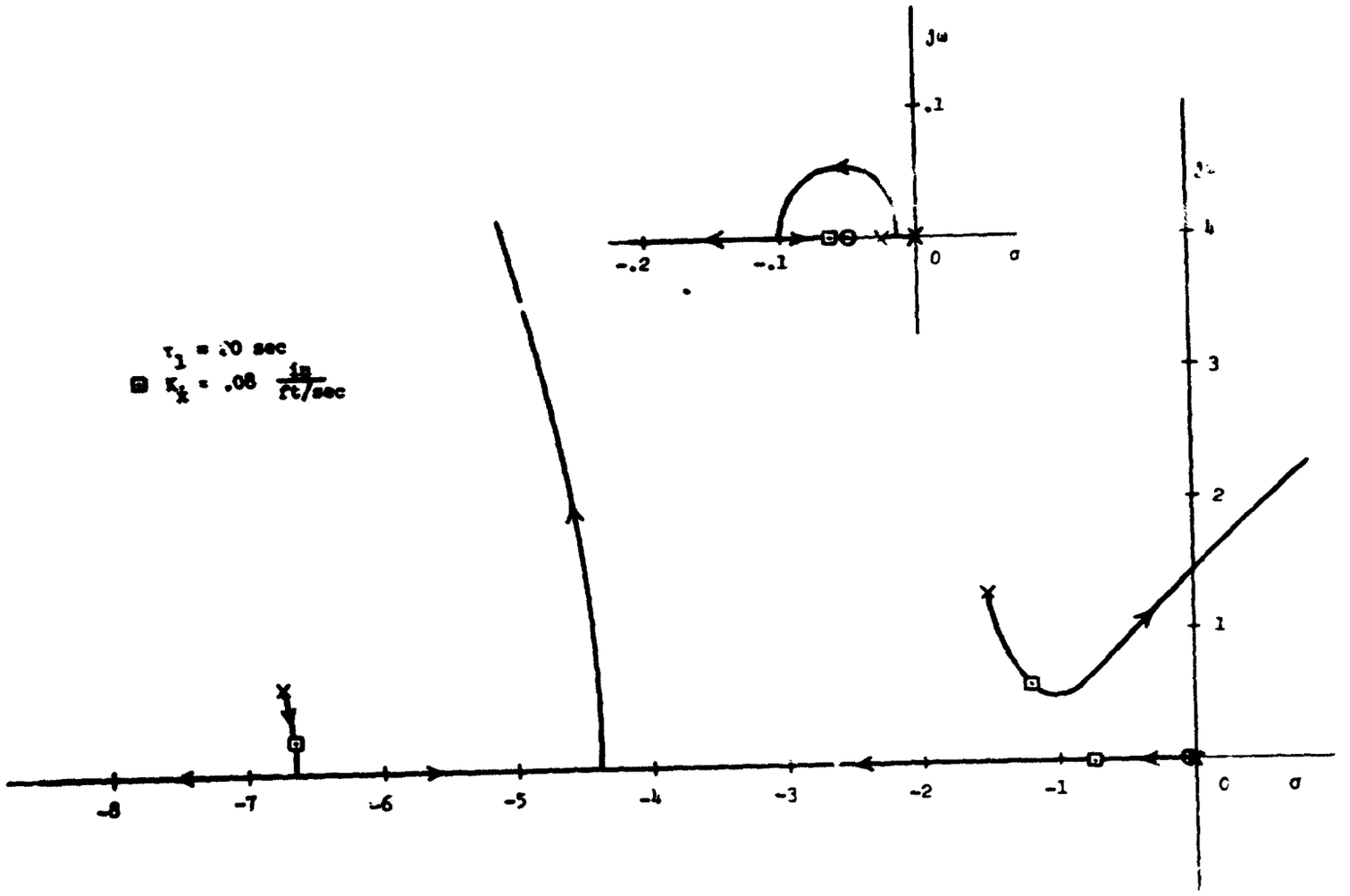

Figure 13.- Root locus for longitudinal velocity control, τ_1 = 20 sec.

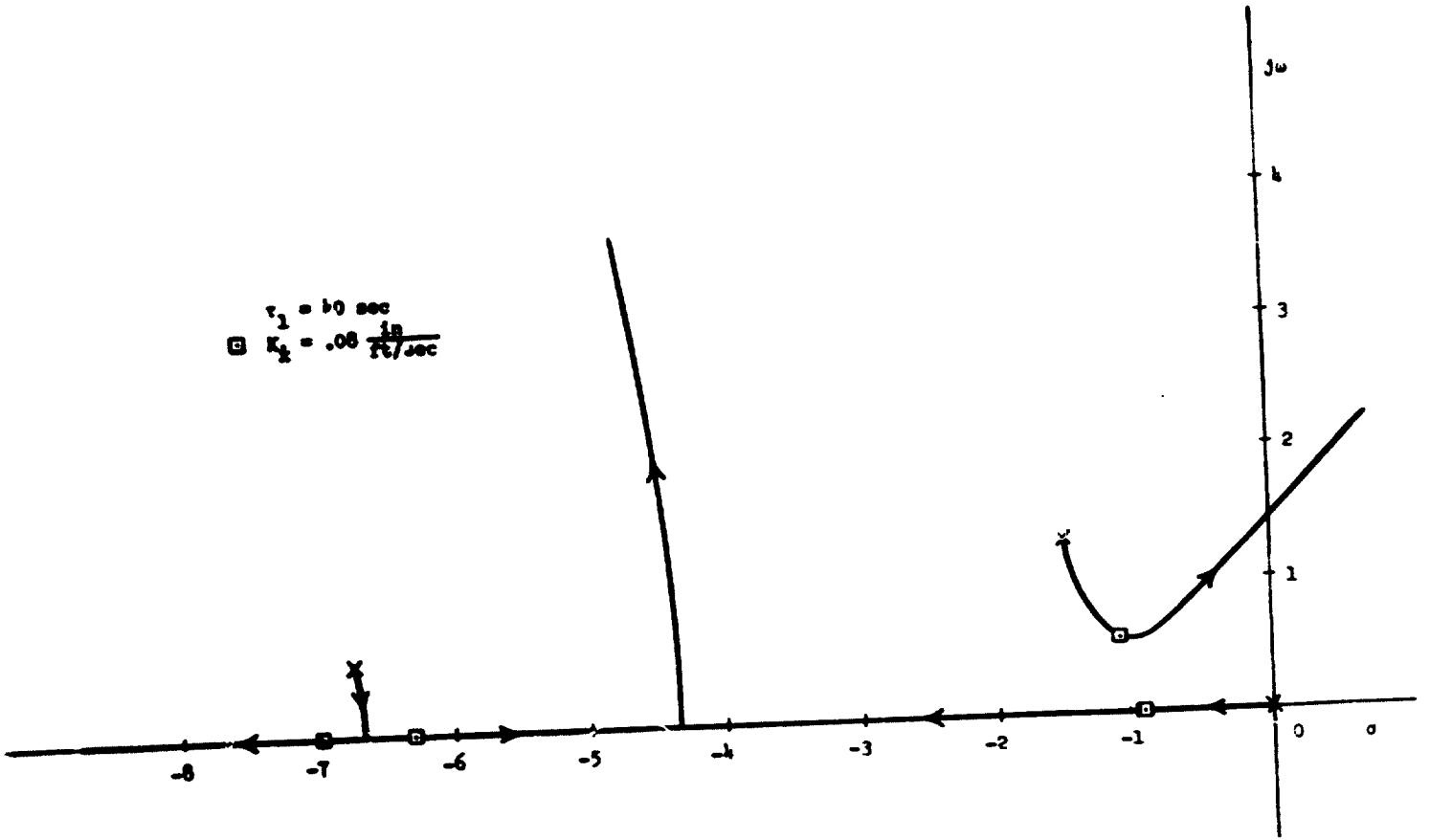

Figure 14.- Root locus for longitudinal velocity control, τ_1 = 40 sec.

After setting $\tau_1 = 40$ sec, choosing the loop gain, $K_{\dot{x}}$, was a straightforward matter. As shown in figure 15, the time response for $K_{\dot{x}} = 0.08 \frac{in}{ft/sec}$ reaches 95 percent of the commanded value within 5 to 6 seconds and is very nearly critically damped. This response is approximately third-order with one real root and a pair of complex roots as indicated in figure 14.

It is noted here that quicker, well damped velocity responses were obtainable with higher loop gains and with additional stabilization terms proportional to pitch attitude and pitch rate. However, a more rapid velocity response was not considered to be either necessary or desirable, based on results of the simulator evaluation. In general, though, these additional stabilization terms might be required to provide a sufficiently quick, well damped velocity response, depending on the attitude response characteristics of the vehicle. It should be kept in mind that the case analyzed here is unique because of its highly stabilized attitude dynamics.

Lastly, control of longitudinal position is considered. Having the velocity control dynamics specified by having selected $K_{\dot{x}} = 0.08 \frac{in}{ft/sec}$ and $\tau_1 = 40$ sec, the position-loop gain, K_x, remains to be determined. The closed-loop roots of the velocity control-loop become the open-loop poles of the position-control loop as indicated in figure 16. Again, the time-response to a step input was used to select the loop gain. It was determined in conjunction with the simulator evaluation that the position response should be nearly critically damped and should attain 95 percent of the commanded

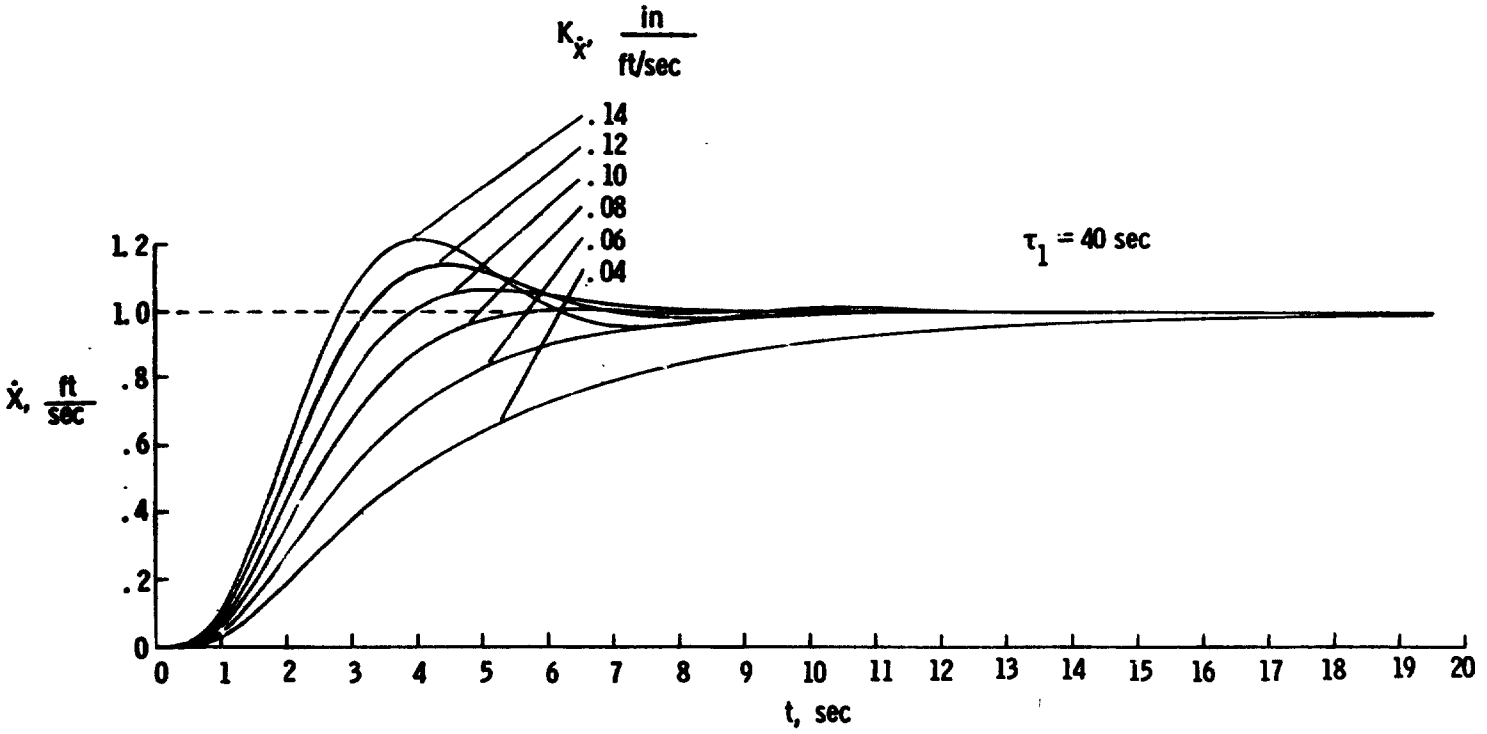

Figure 15.- Longitudinal velocity time response to step command for various $K_{\dot{x}}$.

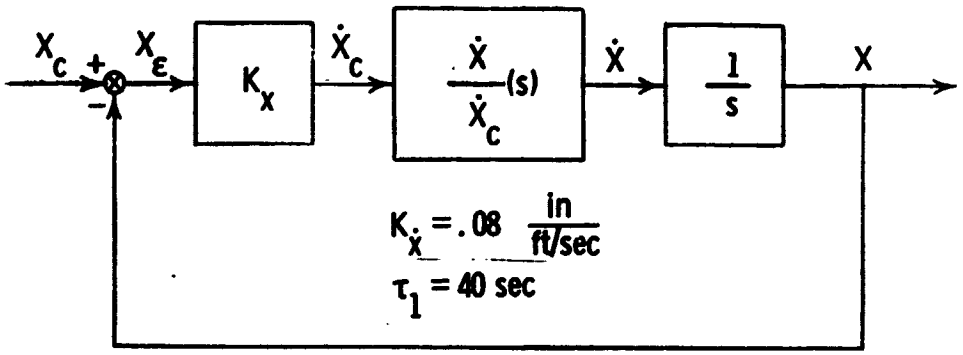

where $$\frac{\dot{X}}{\dot{X}_c}(s) = \frac{68.6}{(s + 6.91)(s + 6.27)(s + .94)(s + 1.12 + j.57)(s + 1.12 - j.57)}$$

$$\frac{\dot{X}}{\dot{X}_c}(s) = \frac{68.6}{s^5 + 16.4s^4 + 88.9s^3 + 188.s^2 + 179.s + 68.6}$$

Figure 16.- Longitudinal position control loop.

position within 15 to 20 seconds. As shown in figure 17, the time response for the selected position-gain, $K_x = 0.14 \frac{ft/sec}{ft}$, satisfies the criterion. Finally, the longitudinal position-control root-locus plot in figure 18 shows that the dominant roots are simply a pair of complex poles with high damping which originate from the integration of velocity-to-position and the dominant real-root of the velocity response.

To develop an appreciation for the sensitivity of the system response to variation in the position and velocity gains, K_x and $K_{\dot{x}}$, an analogy to a second-order system can be drawn. Neglecting all the higher-frequency dynamics associated with the velocity control loop, that is, the pilot dynamics and the attitude response, the system can be grossly simplified to a second-order system as drawn in figure 19. And, the familiar second-order parameters ζ, ω_n, and T_s can be determined as functions of the position and velocity gains.

$$\omega_n \sim \sqrt{K_x K_{\dot{x}}}$$

$$\zeta \sim \sqrt{\frac{K_{\dot{x}}}{K_x}}$$

The settling time, T_s, is the time required for the response to settle within 2 percent of the steady-state.

$$T_s = \frac{4}{\zeta\omega_n}, \quad T_s \sim \frac{1}{K_{\dot{x}}}$$

Thus, to maintain approximately the same damping, if one of the gains were varied, the other would also have to be changed to keep the ratio $\frac{K_{\dot{x}}}{K_x}$ constant. And, if it were desired to halve the response time and

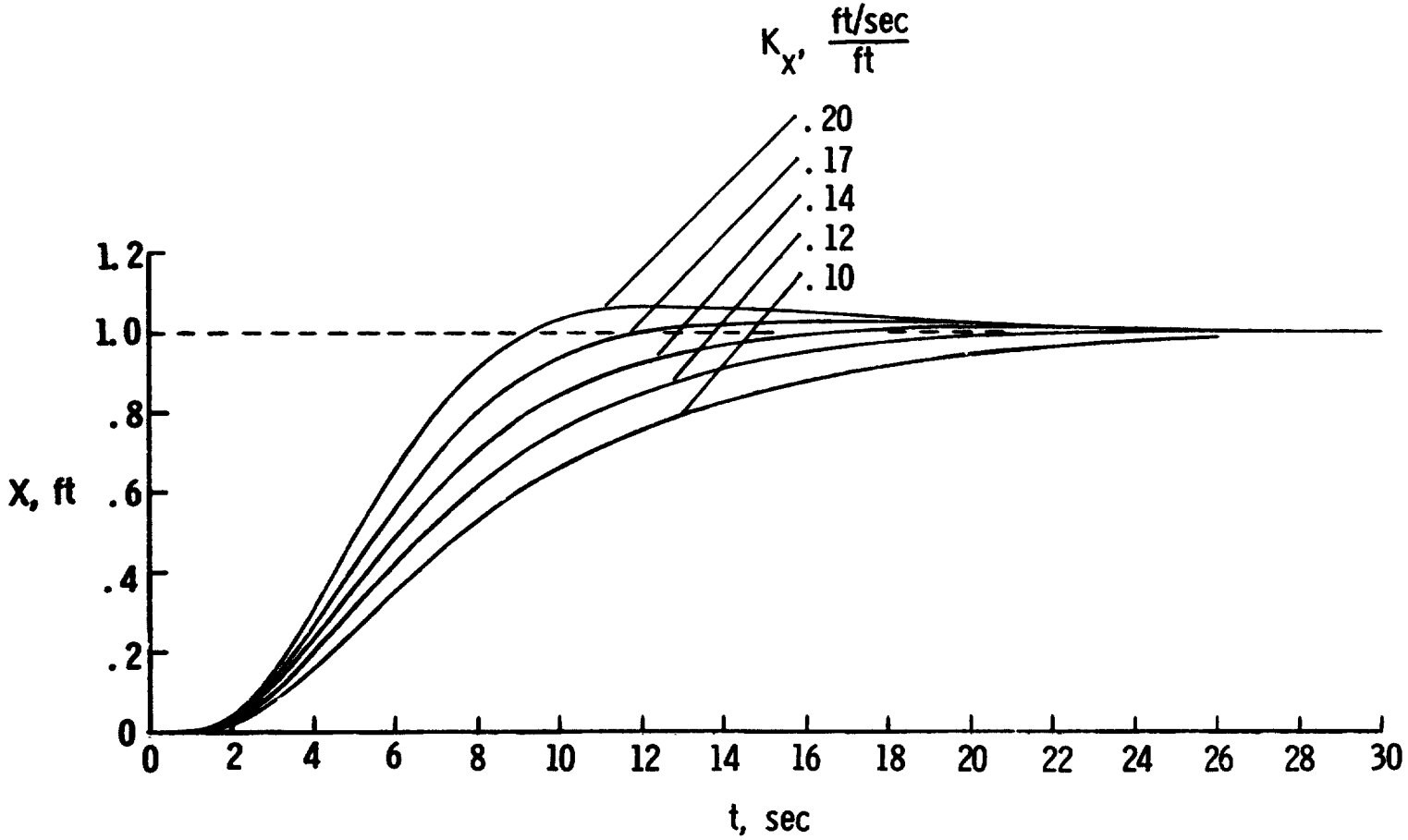

Figure 17.- Longitudinal position time response to step command for various K_x.

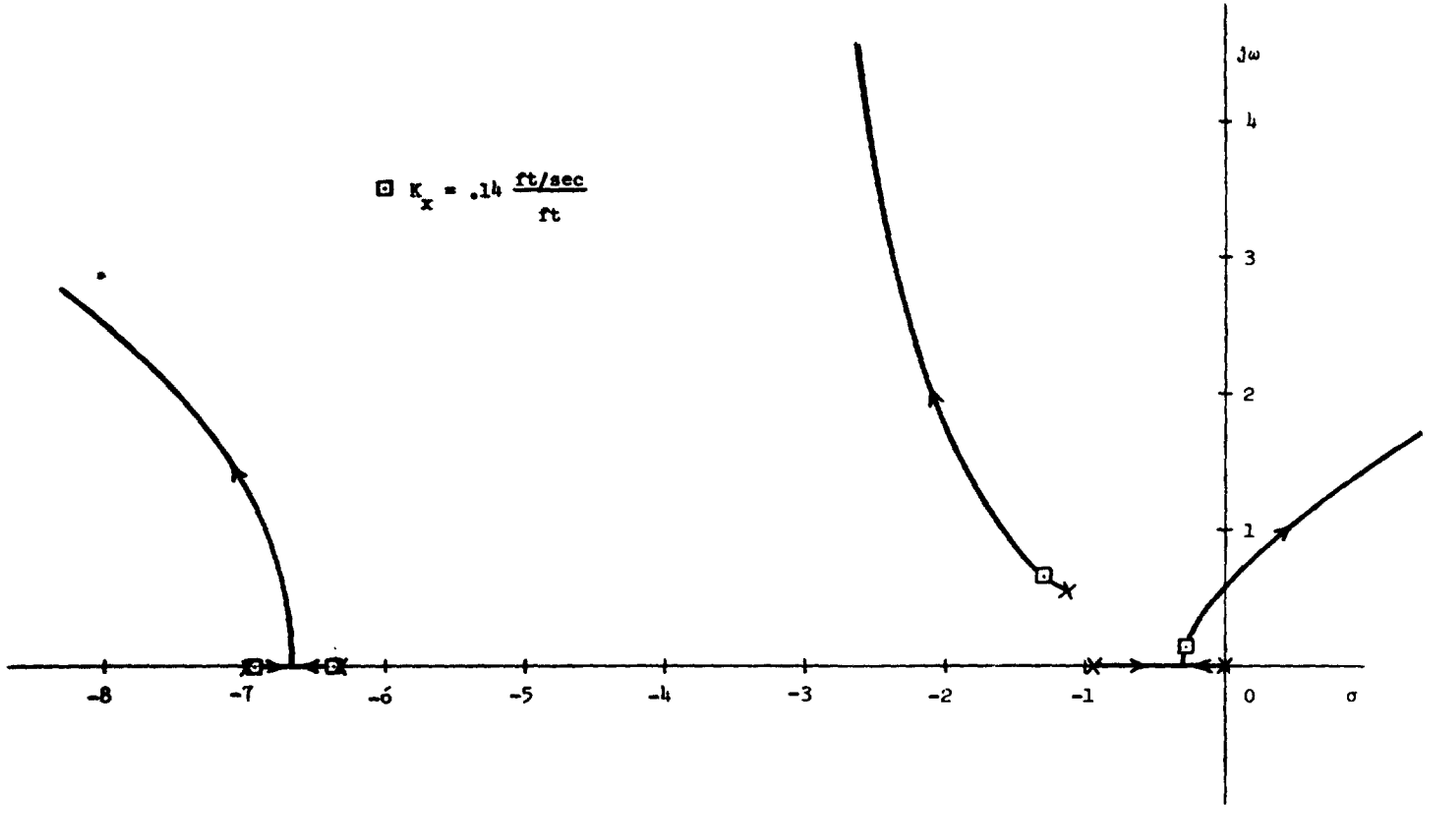

Figure 18.- Root locus for longitudinal position control.

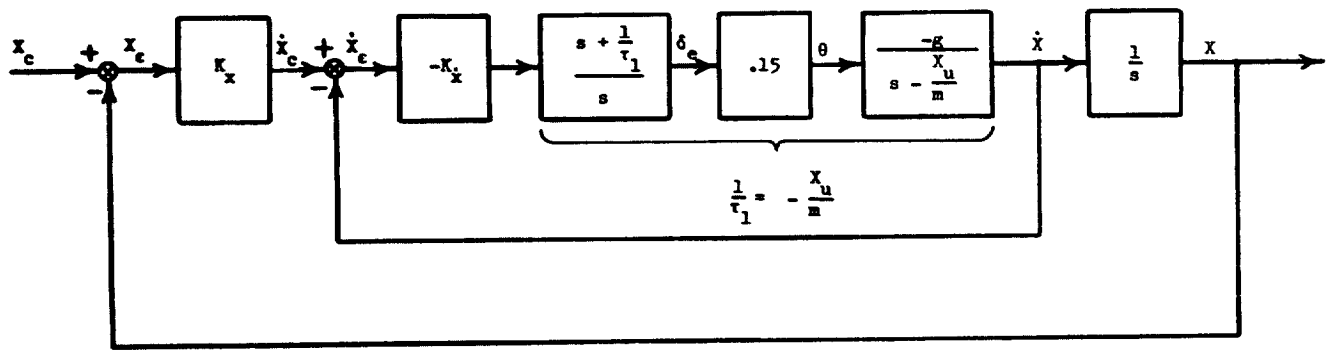

$$\frac{x}{x_c}(s) = \frac{(4.83\ K_x\ K_{\dot{x}})}{s^2 + (4.83\ K_{\dot{x}})s + (4.83\ K_x\ K_{\dot{x}})}$$

$$\frac{x}{x_c}(s) = \frac{\omega_n^2}{s^2 + 2\zeta\omega_n s + \omega_n^2}$$

Figure 19.- Simplification of longitudinal control axis to analogous second-order system.

keep the same damping, then both of the gains would have to be approximately doubled.

Vertical Control Axis

A block diagram of the vertical control axis is presented in figure 20. The same pilot model, of course, is still valid. Longitudinal coupling effects, such as, flare due to changes in pitch attitude, hence angle of attack, and variation of power control trim position with airspeed are regarded as disturbances and are neglected here to permit single input-output type analysis. As in the longitudinal-control axis, the power-control position signal is washed out to prevent steady-state error due to a step, or constant, command for the vertical velocity control loop. Again, the washout time constant, τ_2, is set equal to the time constant of the drag-damping response of the vehicle, $\frac{1}{\left(\frac{-Z_w}{m}\right)}$, to effect a pole-zero cancellation and thus result in a lower-order system. The vertical velocity time response to a step command is given in figure 21. As clearly indicated by the root locus in figure 22, the velocity response is primarily a first-order response for moderate loop gains and then becomes a second-order, underdamped response for much higher gains. A value of $K_{\dot{z}} = 0.08 \frac{in}{ft/sec}$ was judged to provide a satisfactory velocity response, according to the time response criteria mentioned previously. The time response and root locus plots for altitude, or position, control, with $\tau_2 = \frac{1}{\left(\frac{-Z_w}{m}\right)} = 2.5$ sec

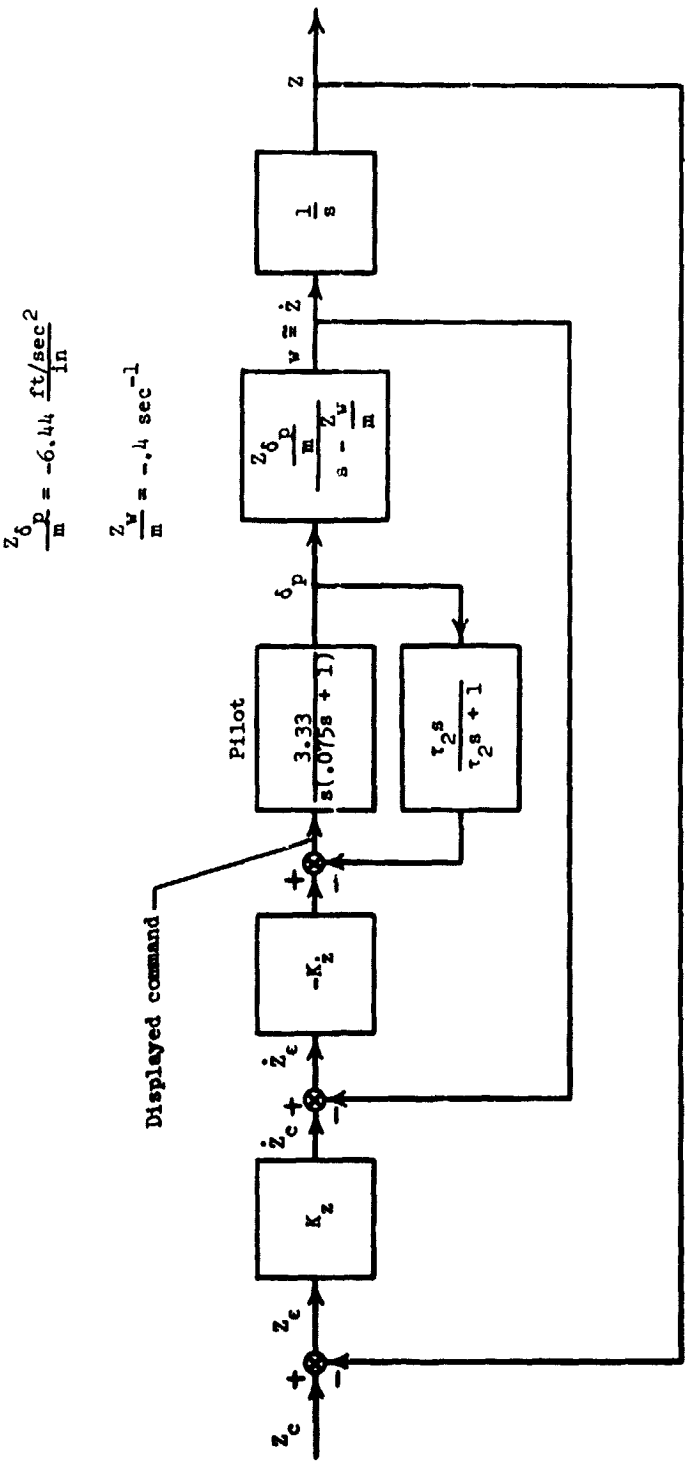

Figure 20.- Vertical control axis.

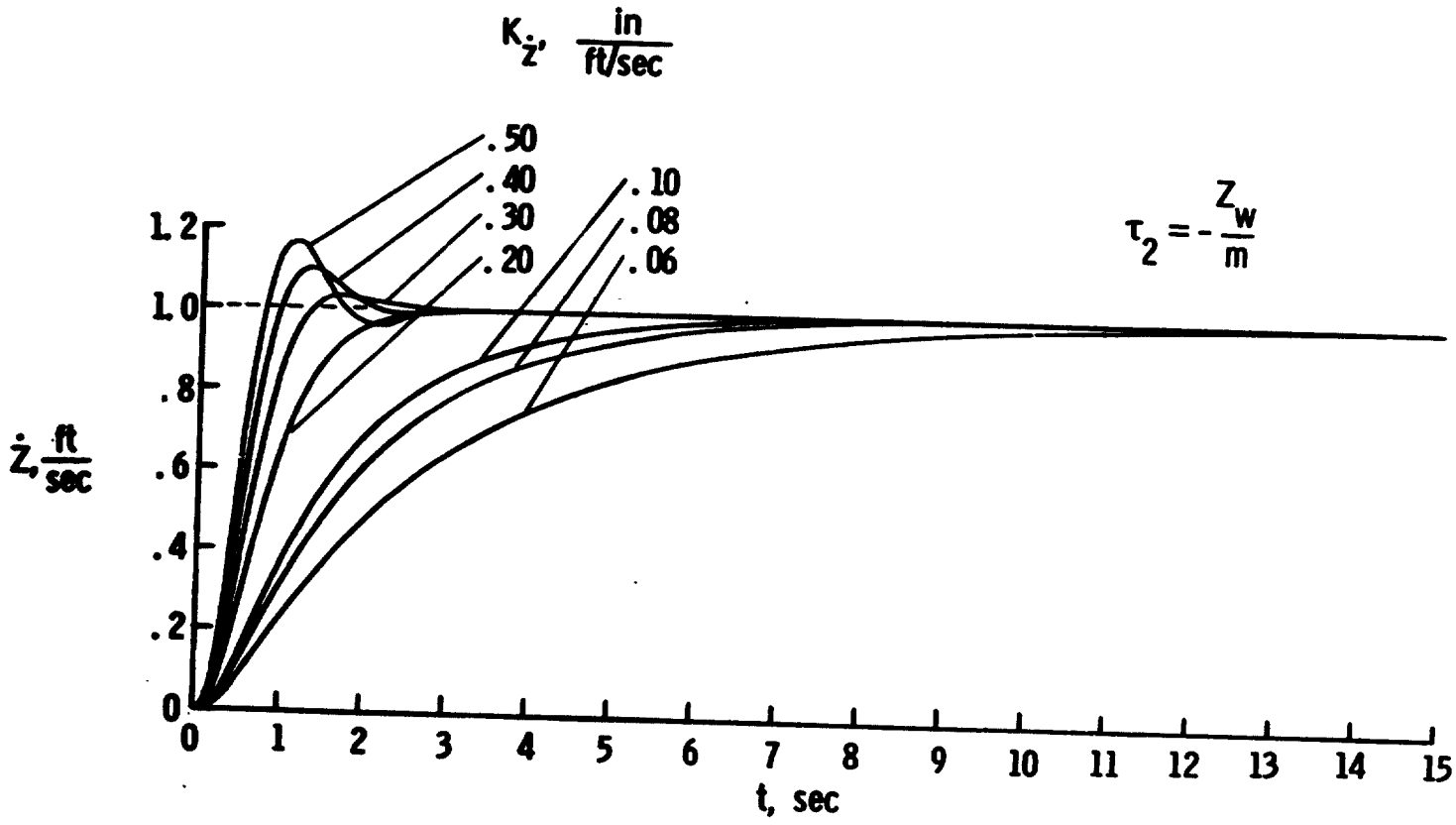

Figure 21.- Vertical velocity time response to step command for various $K_{\dot{z}}$.

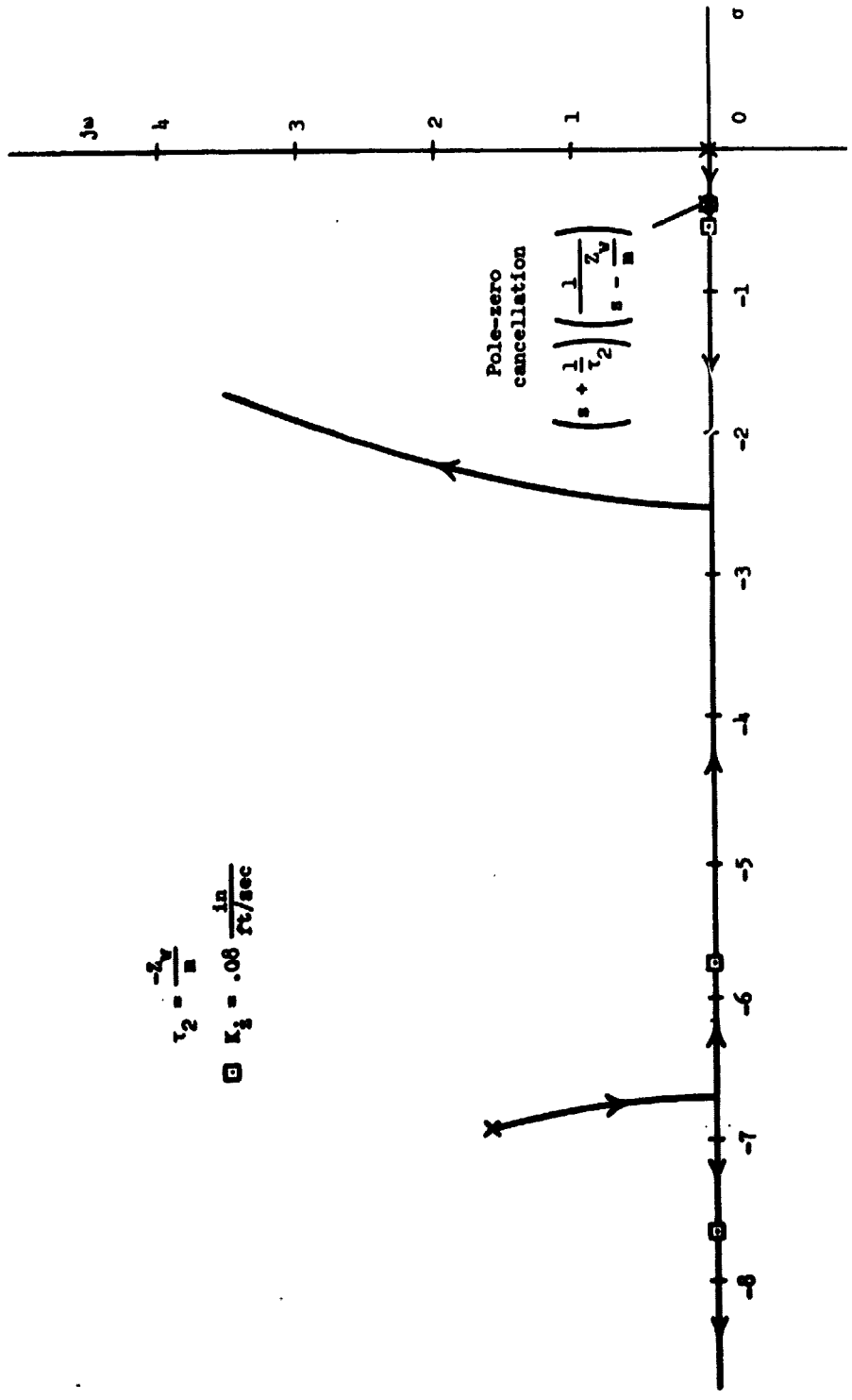

Figure 22.- Root locus for vertical velocity control.

and $K_{\dot{z}} = 0.08 \frac{in}{ft/sec}$, are presented in figures 23 and 24. Selecting $K_z = 0.17 \frac{ft/sec}{ft}$ ensures that the altitude time response, essentially a second-order, well damped response, will satisfy the specified criteria for position control.

Lateral Control Axis (Heading Hold)

The lateral control axis with the heading hold mode is given in figure 25. It has been assumed that the heading of the aircraft is constant and that the difference between the heading of the aircraft and the runway centerline is a small angle. This axis is very similar indeed to the longitudinal control axis. In fact, when the lateral stick washout term, τ_3, is set equal to $\frac{1}{\left(\frac{-Y_v}{m}\right)}$, with the resulting pole-zero cancellation, the control problem becomes nearly identical to that of the longitudinal control axis. The previous work is not repeated here as it is clear that the same gains, $K_{\dot{y}} = 0.08 \frac{in}{ft/sec}$ and $K_y = 0.14 \frac{ft/sec}{ft}$, will provide the desired velocity and position response to step commands.

Lateral Control Axis (Turn Following)

In the turn following mode, the heading of the aircraft automatically changes to produce a coordinated turn which is brought about by holding a bank angle. The dynamics of the lateral control axis for the turn following mode are somewhat complex compared to the previous cases since this mode involves coupling between roll, yaw, and sideslip. The body-axis equations together with the body axis-to-inertial axis

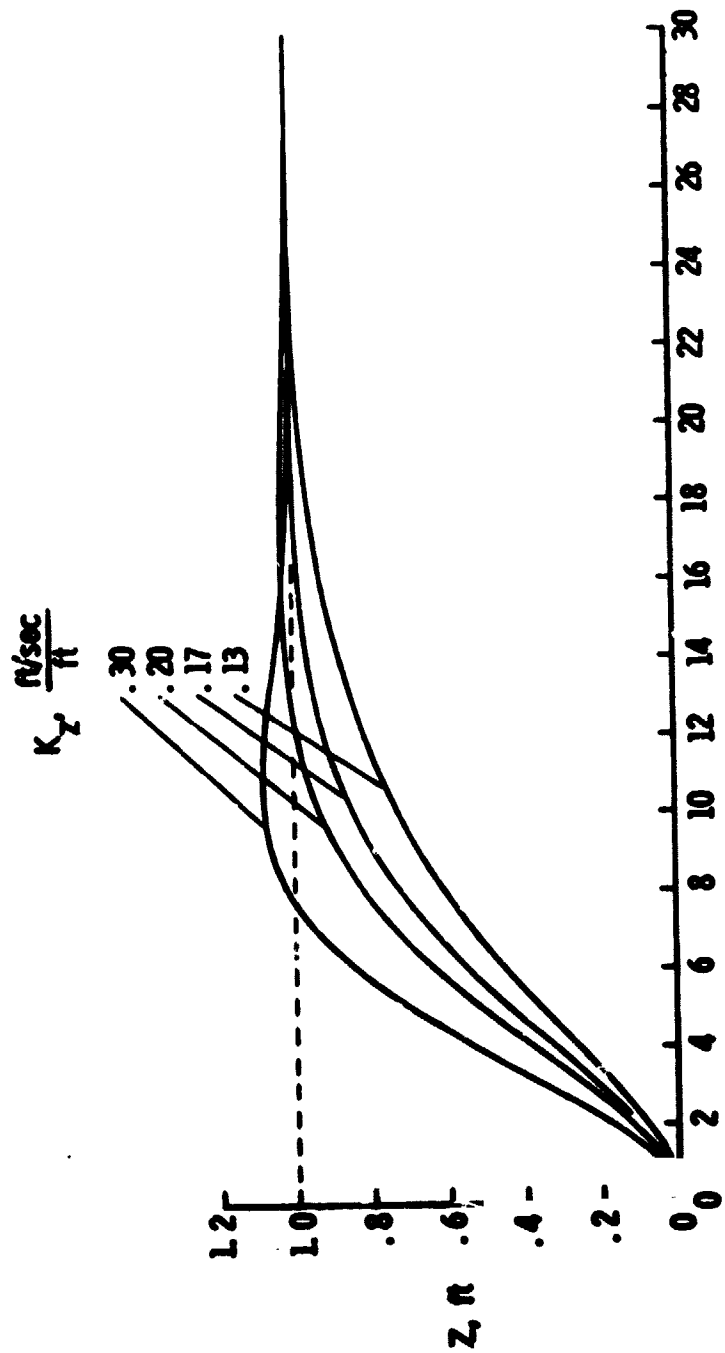

Figure 23.- Altitude time response to step command for various K_z.

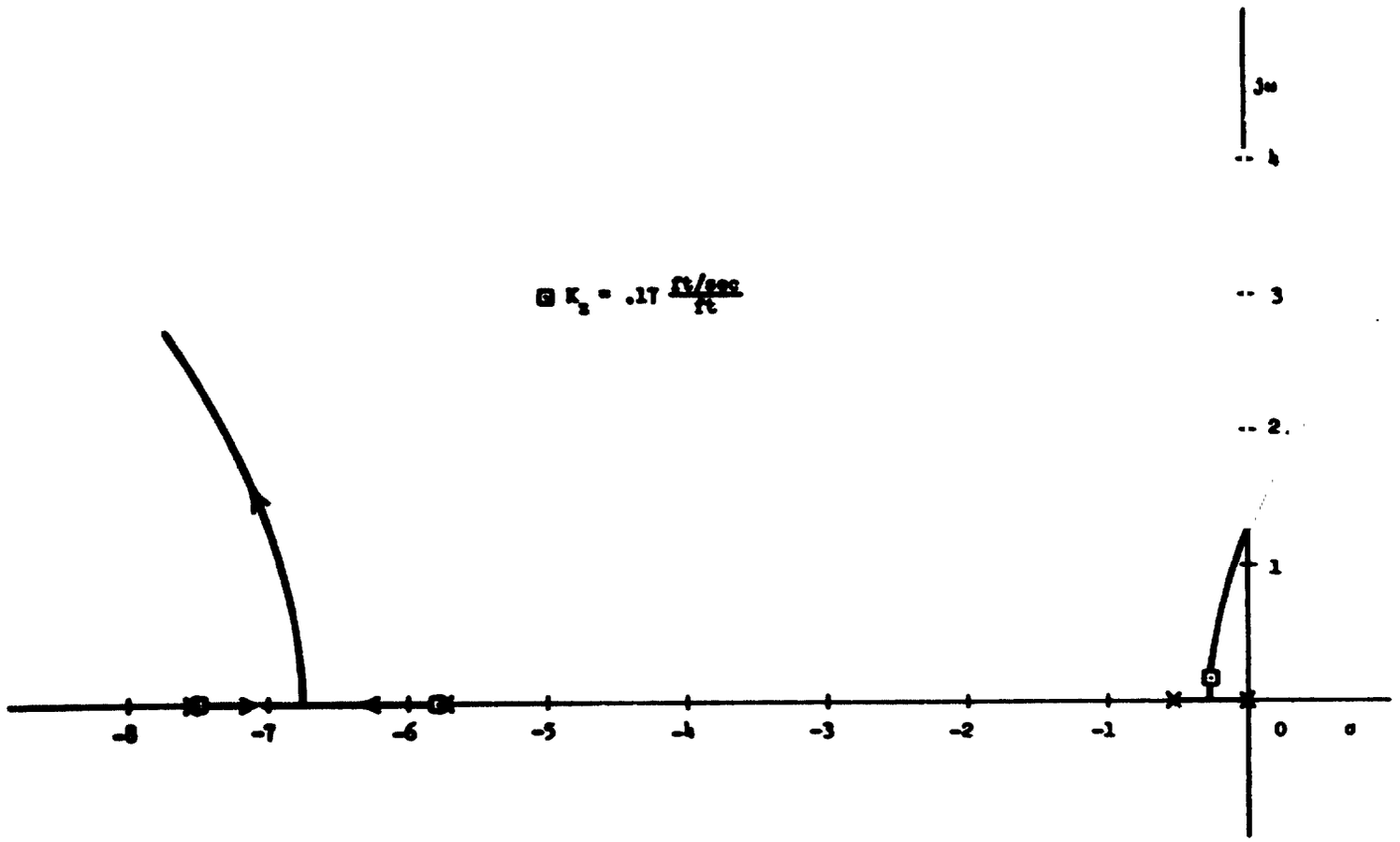

Figure 24.- Root locus for altitude control.

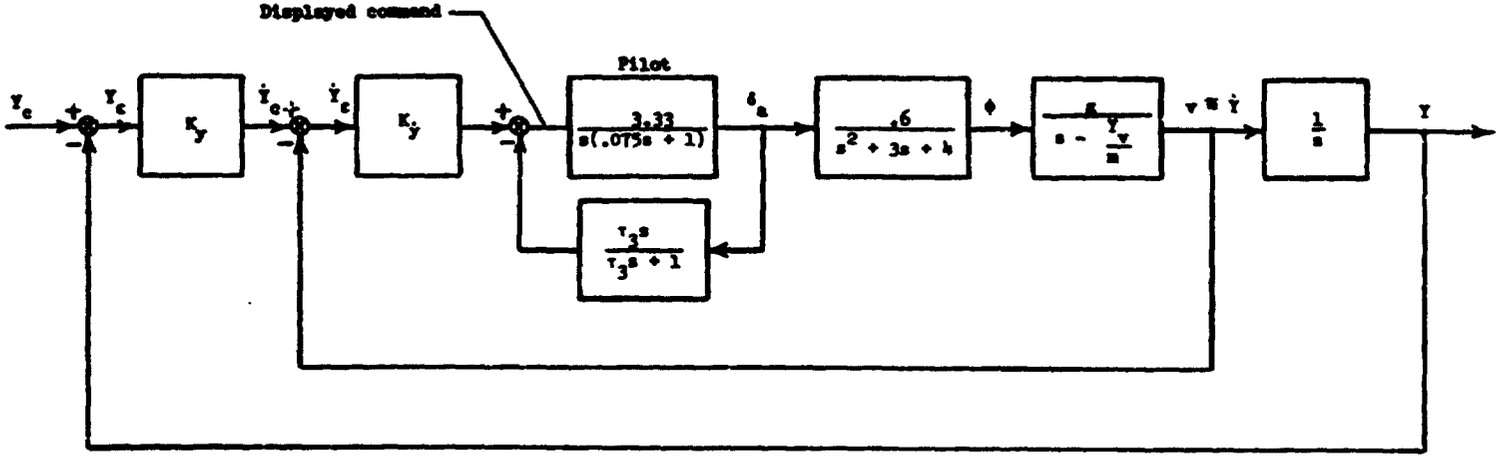

Figure 25.- Lateral control axis (heading hold).

relationship are used here to determine the Laplace transform for $\frac{\dot{Y}}{\delta_a}(s)$ which is needed for the closed-loop analysis.

The body-axis equations are:

$$\dot{p} = \frac{L_p}{I_x} p + \frac{L_\phi}{I_x} \phi + \frac{L_{\delta_a}}{I_x} \delta_a$$

$$\dot{r} = \frac{N_r}{I_z} r + \frac{N_v}{I_z} v + \frac{N_{\delta_a}}{I_z} \delta_a, \quad (\delta_r = 0.)$$

$$\dot{v} = g \phi + \frac{Y_v}{m} v - u_o r$$

The analysis presented here is for a constant forward speed $u_o = 76$ ft/sec (45 knots). Again, it is assumed that the aircraft heading, in relation to the runway centerline, will be a small angle as drawn in figure 26. The transformation relationship,

$$\dot{Y} = u_o \sin \psi + v \cos \psi,$$

can therefore be reduced to the linear equation

$$\dot{Y} \cong u_o \psi + v.$$

These four equations are rewritten using Laplacian notation and grouped in matrix form.

$$\begin{bmatrix} 0 & s(s + 0.7) & -0.004 & 0 \\ s^2 + 3s + 4 & 0 & 0 & 0 \\ -32.2 & 76s & s + 0.1 & 0 \\ 0 & -76 & -1 & s \end{bmatrix} \begin{bmatrix} \phi(s) \\ \psi(s) \\ v(s) \\ y(s) \end{bmatrix} = \begin{bmatrix} 0.065 \\ 0.6 \\ 0 \\ 0 \end{bmatrix} \delta_a(s)$$

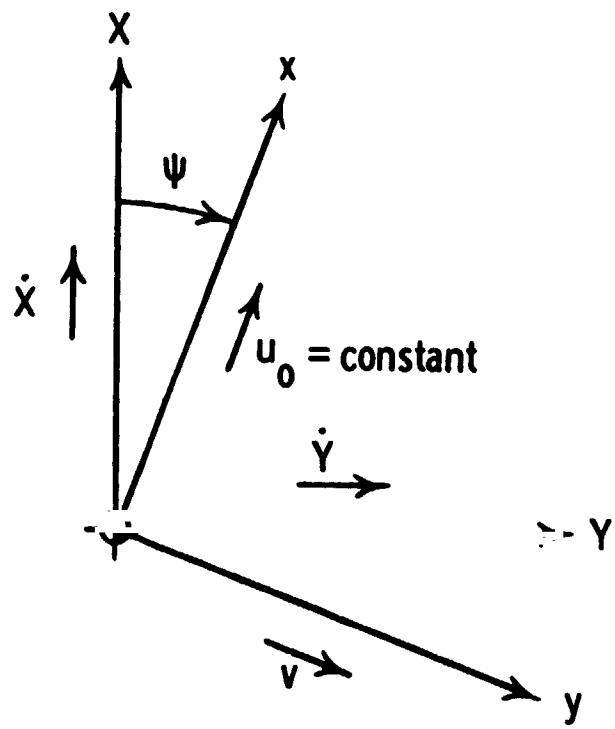

Figure 26.- Body to inertial axis transformation assumed for turn following.

Cramer's Rule is then applied to obtain

$$\frac{\dot{Y}}{\delta_a}(s) = \frac{19.8\,(s^2 + 0.70\,s + 0.40)}{s(s^2 + 3\,s + 4)(s^2 + 0.8\,s + 0.57)}$$

The pole-zero diagram for this transfer function is given in figure 27. The higher frequency complex poles represent the roll attitude response while the other complex poles and zeros appear to nearly cancel one another. The remaining integration is due to the fact that for a coordinated turn, $v \cong 0$, and the turn rate is proportional to bank angle, $\dot{\psi} \cong \frac{g}{u_o}\phi$. Thus, $\dot{Y} \cong u_o\psi$, or $\dot{Y}(s) \cong \frac{g\phi(s)}{s}$.

The lateral control axis for the turn following mode is drawn in figure 28. For this case, a pure integration is present in the feed-forward path of the velocity control loop, and, therefore, there will be no steady-state error due to a step command, and washout will not be required here. The lateral velocity and position responses to step commands, with the corresponding root locus plots, are presented in figures 29, 30, 31, and 32. The same lateral control axis gains that were selected for the heading hold mode, $K_{\dot{y}} = 0.08\ \frac{in}{ft/sec}$ and $K_y = 0.14\ \frac{ft/sec}{ft}$, were also found to be satisfactory for turn following, as indicated by the time response plots. This result was beneficial in actually implementing the flight-director logic since the complexity of switching the gains as a function of yaw mode was thereby avoided.

$$\frac{\dot{Y}}{\delta_a}(s) = \frac{19.8(s^2 + .76s + .40)}{s(s^2 + 3s + 4)(s^2 + .8s + .37)}$$

$$\frac{\dot{Y}}{\delta_a}(s) = \frac{19.8(s + .38 + j.50)(s + .38 - j.50)}{s(s + 1.5 + j1.32)(s + 1.5 - j1.32)(s + .40 + j.46)(s + .40 - j.46)}$$

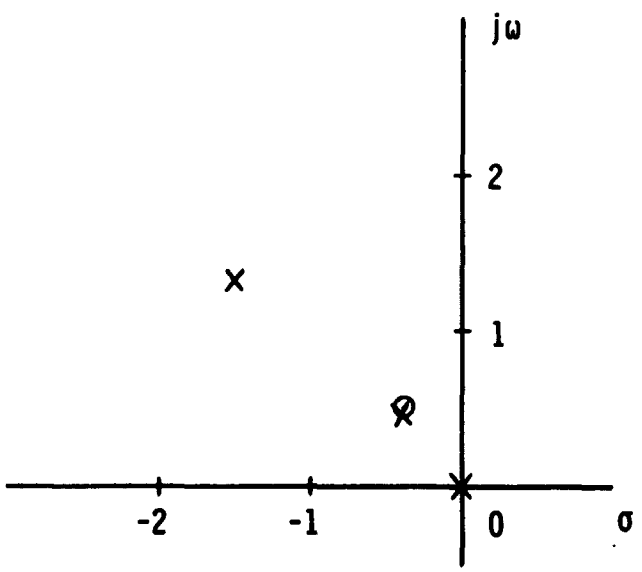

Figure 27.- Transfer function pole-zero diagram for $\frac{\dot{Y}}{\delta_a}(s)$ (turn following).

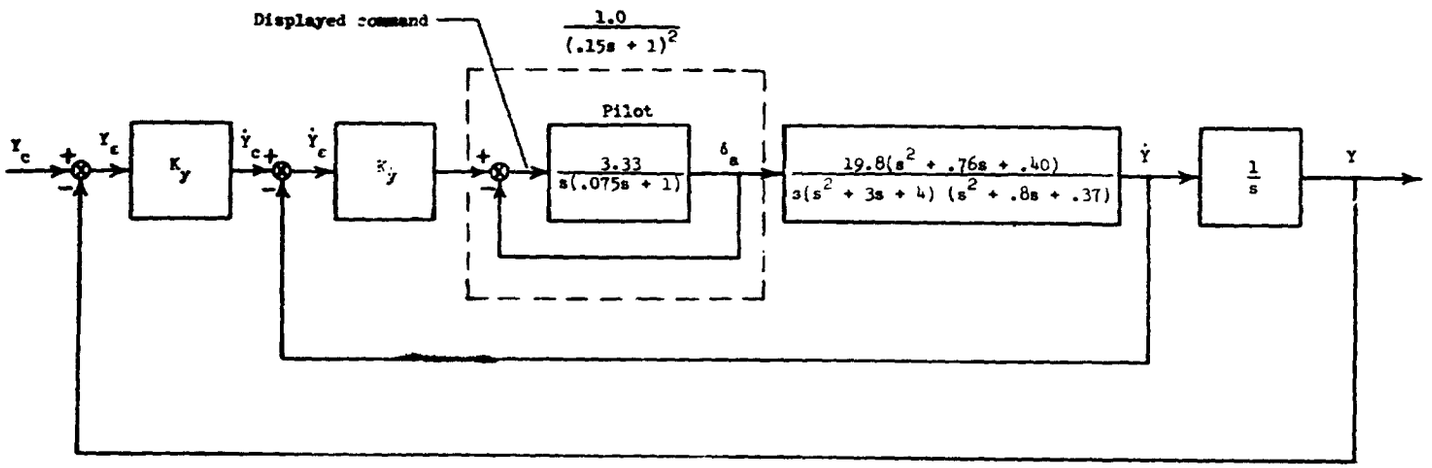

Figure 28.- Lateral control axis (turn following).

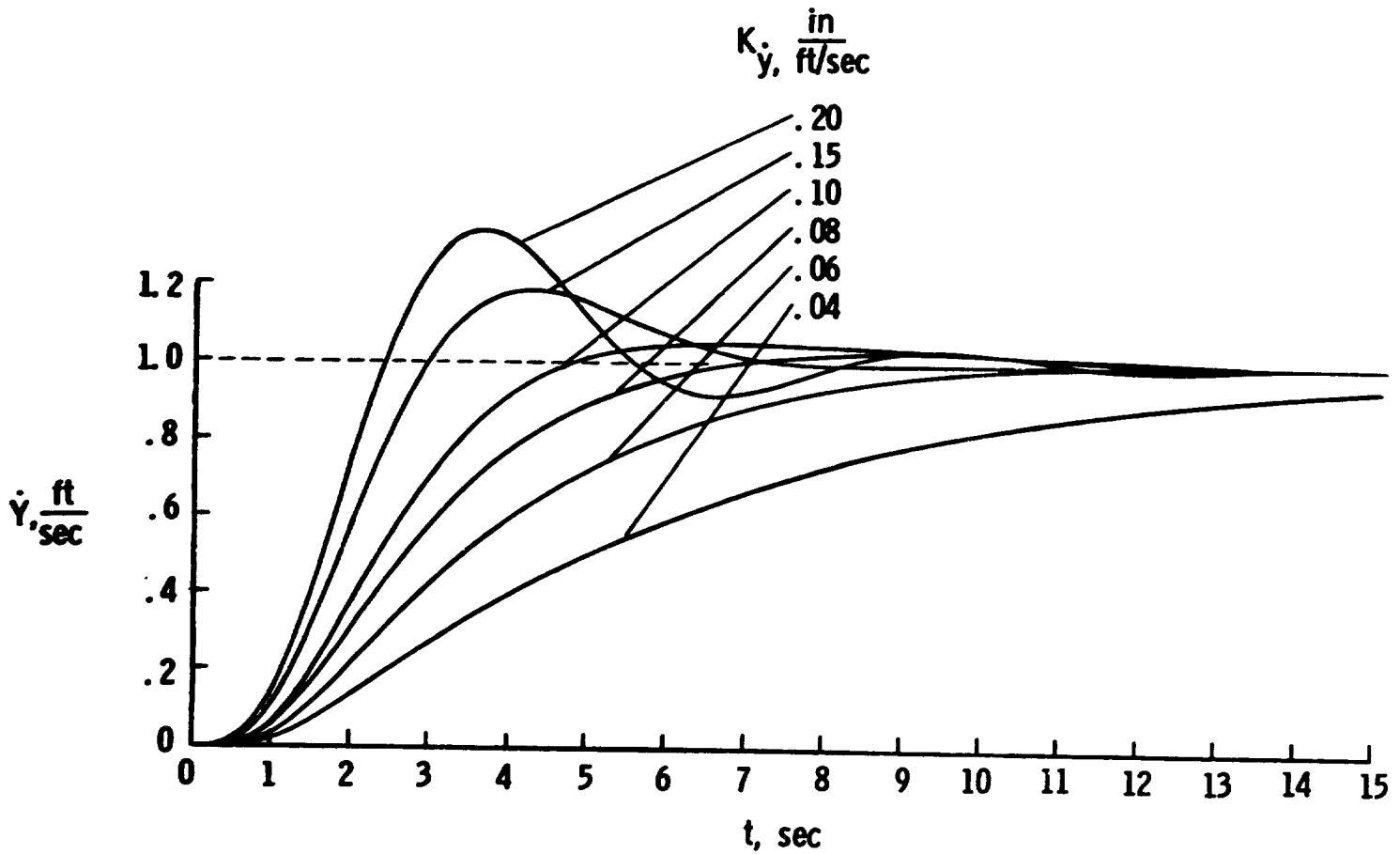

Figure 29.- Lateral velocity time response to step command for various $K_{\dot{y}}$ (turn following).

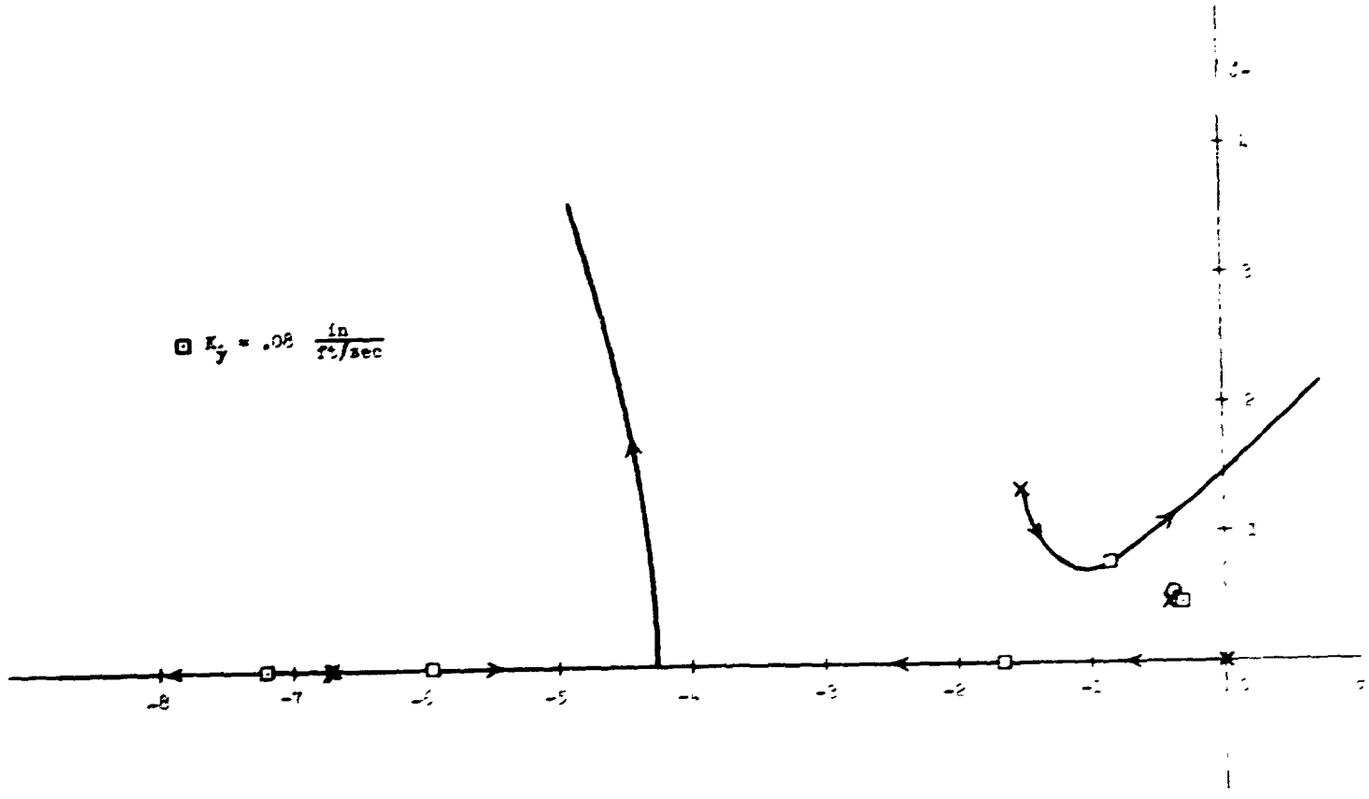

Figure 30.- Root locus for lateral velocity control (turn following).

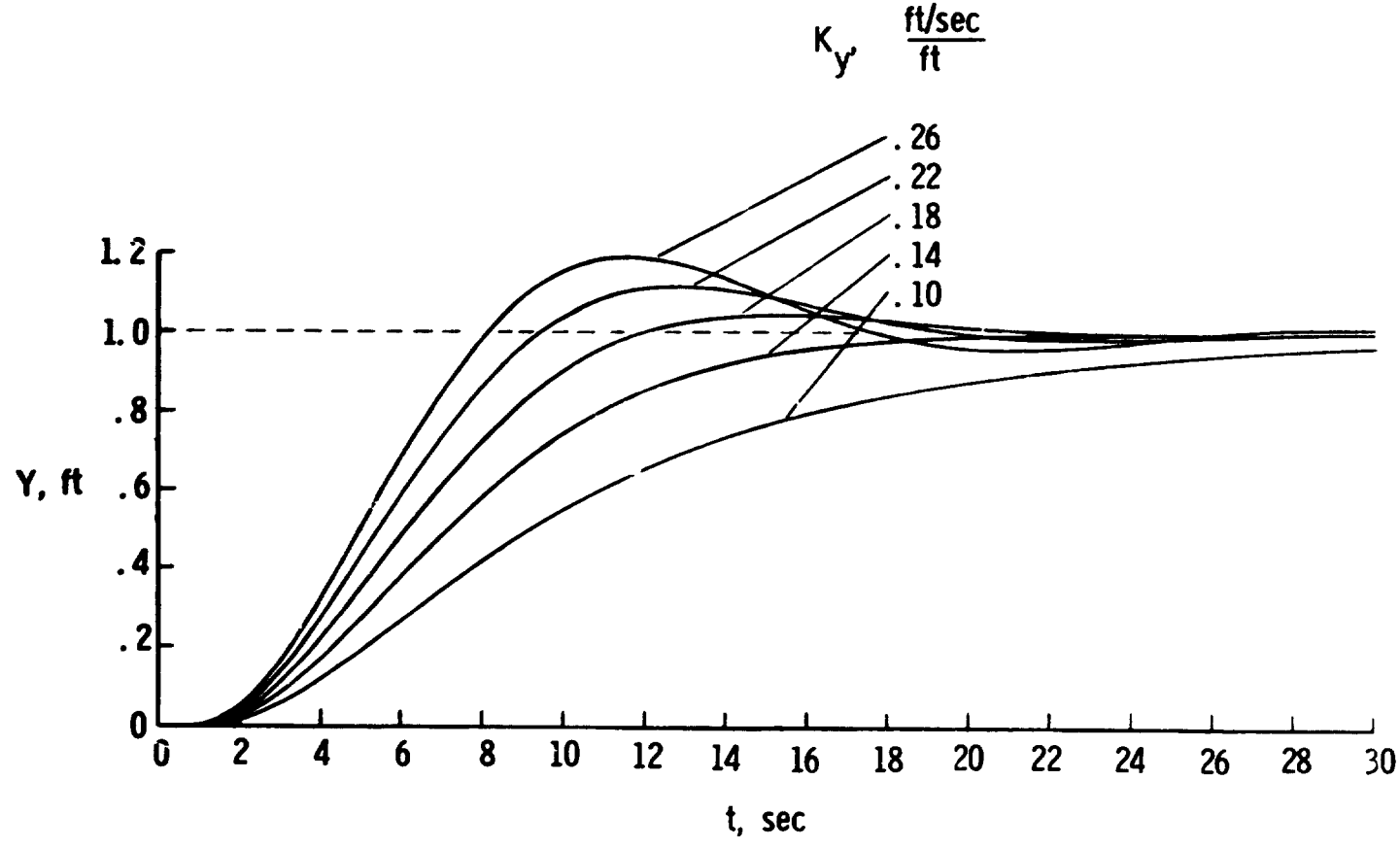

Figure 31.- Lateral position time response to step command for various K_y (turn following).

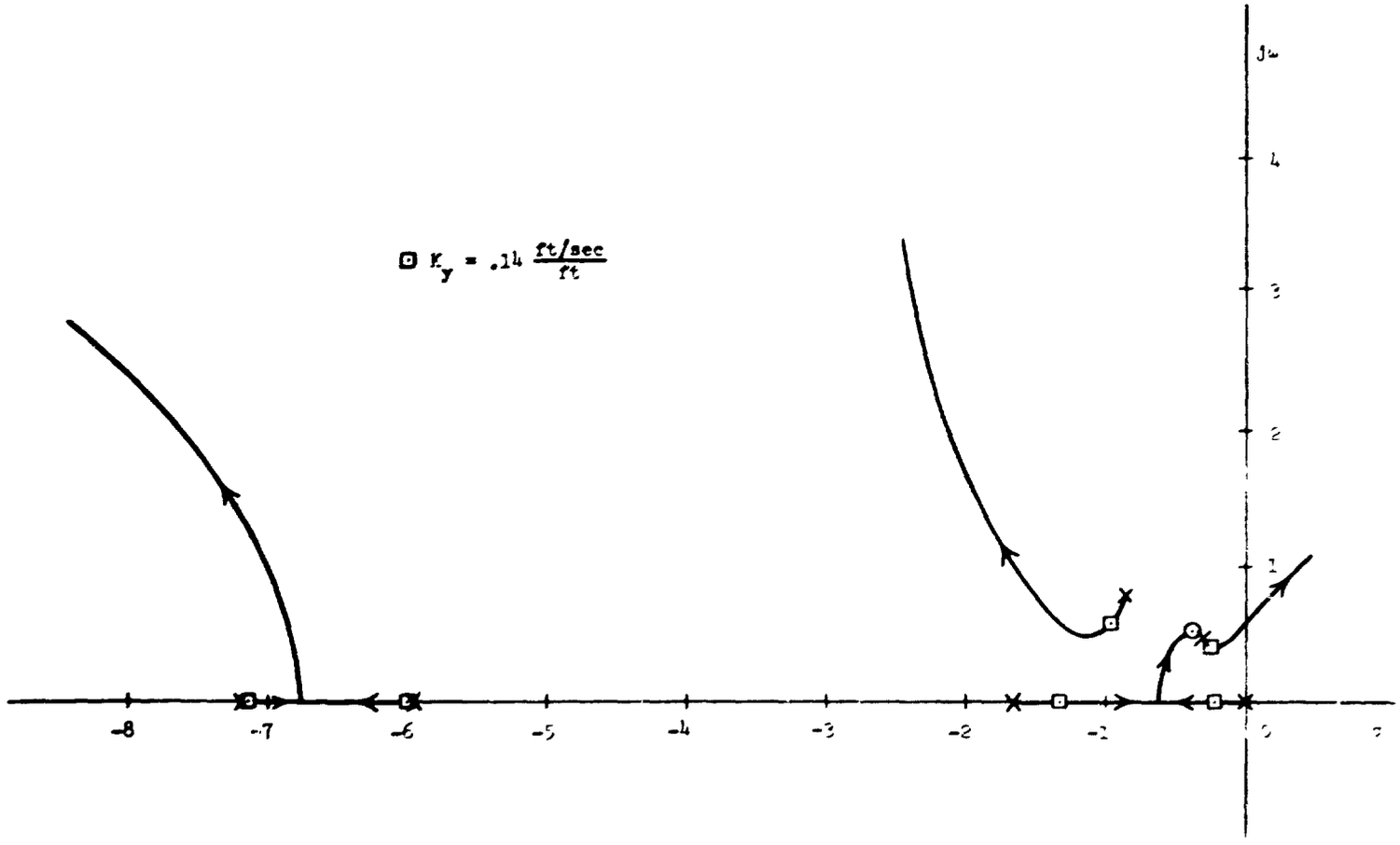

Figure 32.- Root locus for lateral position control (turn following).

CHAPTER IV

FIXED-BASE SIMULATOR EVALUATION

In order to verify and assess the merits of the analytical approach, a fixed-base simulation was used to obtain pilot evaluation of the flight-director control laws. The simulation tests were conducted at the Langley Research Center, National Aeronautics and Space Administration. Subjects who participated in the evaluation included both experienced research test pilots and engineers who had no previous experience as pilots.

Equipment

A photograph of the instrument display panel is shown in figure 33. The Instrument Landing System (ILS) Indicator displayed altitude error (±50 ft) and lateral error (±150 ft) with respect to the nominal flight path. The use of the attitude director indicator was discussed in considerable detail in a previous section. It is pointed out here, though, that the power command needle on the attitude director indicator, which is typically used to display a radio glide slope signal, had a noticeably sluggish response and lead-compensation was required to eliminate this lag. The moving map display provided an indication of longitudinal and lateral position, and aircraft heading. Within 2,500 feet of the center of the landing pad, the map scale factor was 100 $\frac{ft}{in}$, and beyond this distance, the scale factor was 1,000 $\frac{ft}{in}$.

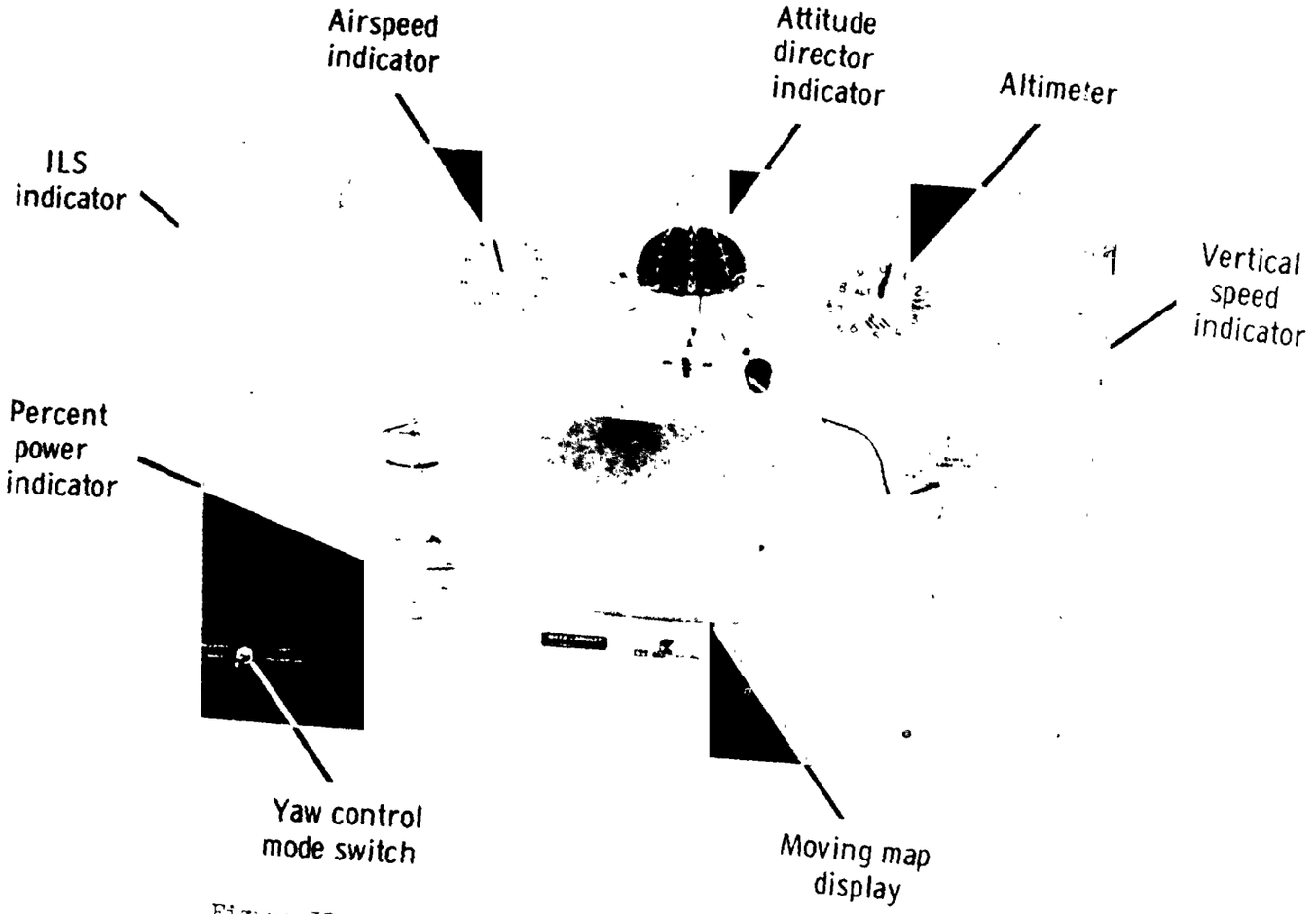

Figure 33.- Fixed-base simulator instrument display panel.

The cockpit controller signals were routed to a Control Data Corporation 6600 series digital computer which provided the real-time solution of the body-axis equations of motion for the helicopter, the transformation equations, and the flight-director control laws. The variables which were displayed on the instrument panel were routed back from the computer to the cockpit. The digital computer performed 32 computations per second and used a second-order Adams-Moulton (2 pass) integration routine. Time histories were obtained using two 8-channel strip-chart recorders.

Simulator Equations

The body-axis equations of motion used to represent the vehicle dynamics are given in table 3. It was assumed here that the high-gain control augmentation system would completely eliminate effects of disturbances and basic vehicle trim changes for the angular degrees of freedom. The power required characteristic was simulated in the vertical degree of freedom by inserting a power-control trim position term as a function of speed, $\delta_{p_o}(u)$. In addition, random wind disturbances were included in the appropriate aerodynamic force and moment terms. The gusts were obtained by passing the output of a random-noise generator through a first-order filter with a break frequency of 10 $\frac{\text{rad}}{\text{sec}}$. An average headwind/tailwind and crosswind, each with a random gust term, were specified in the inertial reference frame, and the body-axis disturbance terms u_g and v_g were obtained by resolving the headwind and crosswind components as a

TABLE 3

FIXED-BASE SIMULATOR EQUATIONS

A. Body-Axis Equations of Motion

$$\dot{q} = \frac{M_q}{I_y} q + \frac{M_\theta}{I_y} \theta + \frac{M_{\delta_e}}{I_y} \delta_e$$

$$\dot{p} = \frac{L_p}{I_x} p + \frac{L_\phi}{I_x} \phi + \frac{L_{\delta_a}}{I_x} \delta_a$$

$$\dot{r} = \begin{cases} \frac{N_r}{I_z} r + \frac{N_v}{I_z} (\quad + v_g) + \frac{N_{\delta_r}}{I_z} \delta + \frac{N_{\delta_a}}{I_z} \delta & \text{(Turn Following} \\ \frac{N_r}{I_z} r + \frac{N_\psi}{I_z} (\quad - \psi') \quad \text{where} \quad \psi' = \int_o^t \left(0.35 \frac{\text{rad/sec}}{\text{in}}\right) \delta_r \, dt & \text{(Heading Hold} \end{cases}$$

$$\dot{u} = -g\theta + \frac{X_u}{m} (u + u_g) + vr - wq$$

$$\dot{v} = g\phi + \frac{Y_v}{m} (v + v_g) - ur + wp$$

$$\dot{w} = \frac{Z_w}{m} (w + w_g) + \frac{Z_{\delta_p}}{m} \left[\delta_p - \delta_{p_o}(u)\right] + uq - vp$$

TABLE 3.- CONCLUDED

B. Body-Axes to Inertial-Axes Transformation Equations

$$\dot{\theta} = q$$

$$\dot{\phi} = p$$

$$\dot{\psi} = r$$

$$\dot{X} = u \cos \psi - v \sin \psi + w\theta \cos \psi + w\phi \sin \psi$$

$$\dot{Y} = u \sin \psi + v \cos \psi + w\theta \sin \psi - w\phi \cos \psi$$

$$\dot{Z} = -u\theta + v\phi + w$$

function of the heading of the aircraft. The vertical wind disturbance term, w_g, was assumed to have a zero average wind component. The amplitudes of the random wind components were adjusted to yield a root-mean-square amplitude of 6.0 $\frac{ft}{sec}$ for gusts in the horizontal plane and 2.0 $\frac{ft}{sec}$ for the vertical gusts.

The transformation equations used to resolve the motions of the aircraft to the inertial reference frame are also presented in table 3. These rather simple expressions were derived from the Euler transformation equations by assuming that the pitch and roll attitudes of the aircraft would be small angles.

Results and Discussion

As mentioned before, each subject was allowed to select whichever sensing he preferred for each of the three command signals. There was actually quite a difference in preferences among the various individuals, although most of the pilots did prefer the conventional inside-out type sensing as indicated in figure 3. Undoubtedly, their previous training greatly influenced this selection. It was found that with very little practice, each of the test subjects was able to respond to commands without hesitation and with a minimum of control reversals regardless of the sensing he had selected.

The sensitivities of the displayed commands which were used, in terms of full-scale displacements, were 3.0 inches for longitudinal and lateral stick commands, and 2.0 inches for the power command. It was discovered that sensitivities over a fairly large

range were acceptable because in centering the command the pilot apparently could readily adjust his gain to that of the display. Furthermore, since the command signals are always kept centered, or nulled, the sensitivity of the displayed command does not have a significant effect on the closed-loop response of any of the outer-loops. For these reasons, the sensitivity of the displayed commands was not considered to be a very critical factor.

The flight-director commands, as they were initially formed, were usable but were oversensitive because of the effective gain controlled-element dynamics. That is, since the inner-loop feedback term was the control position signal itself, the command signal was unnecessarily responsive to pilot control inputs. The result was that instead of being steady, positive commands, the commands were jittery and, therefore, somewhat bothersome. When the high frequency control position terms were omitted from the displayed commands, however, the resulting command signals were more difficult to control and were even less acceptable. It was apparent from this that a high frequency command which could be readily centered by the pilot was preferred, although the gain controlled-element dynamics was too sensitive. A satisfactory compromise was achieved by passing the control position term of the flight-director command through a low-pass filter. It was found that a first-order filter with a time constant of 0.8 seconds resulted in the best flight-director response. Shorter time constants resulted in too sensitive a response and longer time constants resulted in too sluggish a response.

In spite of the modification discussed previously, the theoretical analysis, which included a pilot model based on the assumption of gain controlled-element dynamics, was still believed to be valid since the task of centering the flight-director needle appeared to be accomplished just as readily using the filtered control position feedback. This was substantiated in reference 1 which indicated that for the controlled-element dynamics $\frac{1}{s+1}$ the pilot was able to effectively maintain the same closed-loop dynamic response as for the gain controlled-element dynamics. The pilot transfer function parameters which were obtained in that study for the $\frac{1}{s+1}$ dynamics are listed in table 4.

It should be pointed out that the assumption made here that the control position signals are available does not present a limitation with regard to the practical design of such systems. It is quite possible to synthesize an equivalent filtered control position signal by dynamically combining the appropriate higher frequency vehicle dynamics terms. For instance, by combining pitch and pitch rate terms in this manner, a signal equivalent to the filtered longitudinal stick position was obtained. Since the roll attitude dynamics are identical to pitch, the same is true for the lateral control axis. Similarly, a normal acceleration term can be shown to be equivalent to the washed-out power-control position signal, and, in addition, this term provides quickened information with regard to flare effects due to pitch changes and with regard to the power required characteristic. For this type of reason, in fact, it appears

TABLE 4

MEASURED PILOT TRANSFER FUNCTION PARAMETERS FOR $\frac{1}{s+1}$ CONTROLLED-ELEMENT DYNAMICS

Test Subject	$\frac{\delta}{D}(s) = \frac{K_p(\tau_L s + 1)}{(\tau_I s + 1)^2}$		
	K_p	τ_L	τ_I
Pilot A	0.85	1.08	0.15
Pilot B	0.75	1.25	0.25
Pilot C	0.72	0.5	0.17
Pilot D	0.86	1.3	0.29
Pilot E	1.14	1.14	0.29
Pilot F	0.42	0.67	0.17
Engineer G	0.67	0.67	0.22
Engineer H	1.0	1.0	0.13

advantageous to use shaped higher frequency vehicle dynamics terms in preference to the filtered control position signal itself.

Examination of the resulting flight-director dynamics as designed by the approach taken here, indicates close agreement with the basic contention put forth in reference 10 that the flight-director response to pilot input should approximate $\frac{K}{s}$ -like dynamics. For example, the frequency response plot for the flight-director response to pilot input for longitudinal velocity control is given in figure 34. The $\frac{K}{s}$ - like approximation has been achieved for nearly all frequencies except for very low frequencies. Apparently, the equivalent filtered control position signal yields the proper initial response and allows the pilot to achieve cross-over at a desirable frequency with an acceptable gain. The outer-loops, which are closed through typical automatic control considerations, would normally be expected to yield $\frac{K}{s}$ - dynamics near the cross-over region.

The time response criteria which were used in the analyses were based on pilot comments received during the simulator evaluation. These comments were generally made with regard to the desired aircraft response in correcting for small errors which would typically occur due to wind disturbances or periods of pilot inattention. It was found that the pilot's ability to track the command was not greatly affected by variation of the outer-loop gains, or lower-frequency terms, since this closure was accomplished by manipulation of the higher-frequency terms. The main concern with regard to the outer-loop gains was that the velocity and position responses should,

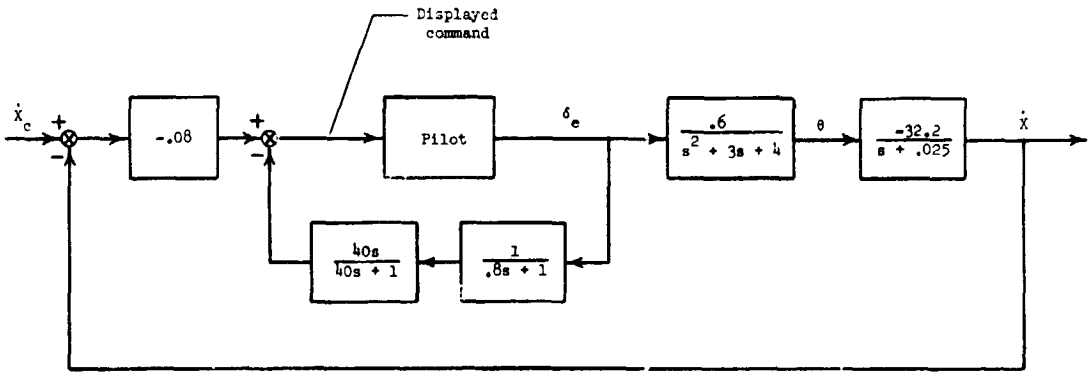

$$\frac{\text{Displayed command}}{\delta_e}(s) = \left(\frac{1}{.8s+1}\right)\left(\frac{40s}{40s+1}\right)(-1) + \left(\frac{.6}{s^2+3s+4}\right)\left(\frac{-32.2}{s+.025}\right)(-1)(-.08)$$

$$= -\frac{(s+.36)(s^2+2.64s+4.28)}{(s+.025)(s^2+3s+4)(.8s+1)}$$

Frequency response

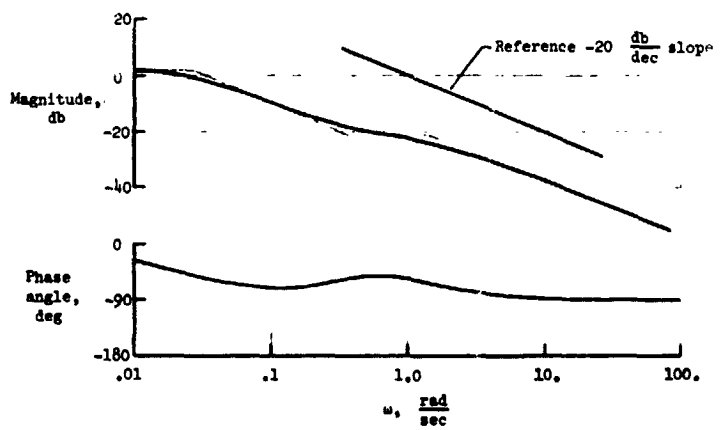

Figure 34.- Flight-director response to pilot control input for longitudinal velocity control.

first of all, be well damped without any appreciable overshoot. The desired quickness of the response seemed to depend on the task. That is, if the task required a great deal of precision, such as maintaining a hover at low altitude, then a fairly quick response, or higher bandwidth system, would be desired. However, for a constant speed approach, where not quite as much accuracy would be necessary, lower gains or a slower response would probably be acceptable. It is noted that the time response criteria used in the analysis corresponded to the more stringent requirements of a precise task.

Time histories for two simulator runs are presented in figures 35 and 36. The first set of time histories is for a 45-knot constant speed approach along a 6-degree glide path, for which the turn following yaw mode had been selected. The other set of time histories corresponds to an instrument hover at an altitude of 50 feet, using the heading hold mode. For both of these runs, the specified average wind had a 6-knot headwind component and a 4-knot crosswind component. The capability of the system in maintaining position, or velocity, in the presence of wind disturbances is evident from these records.

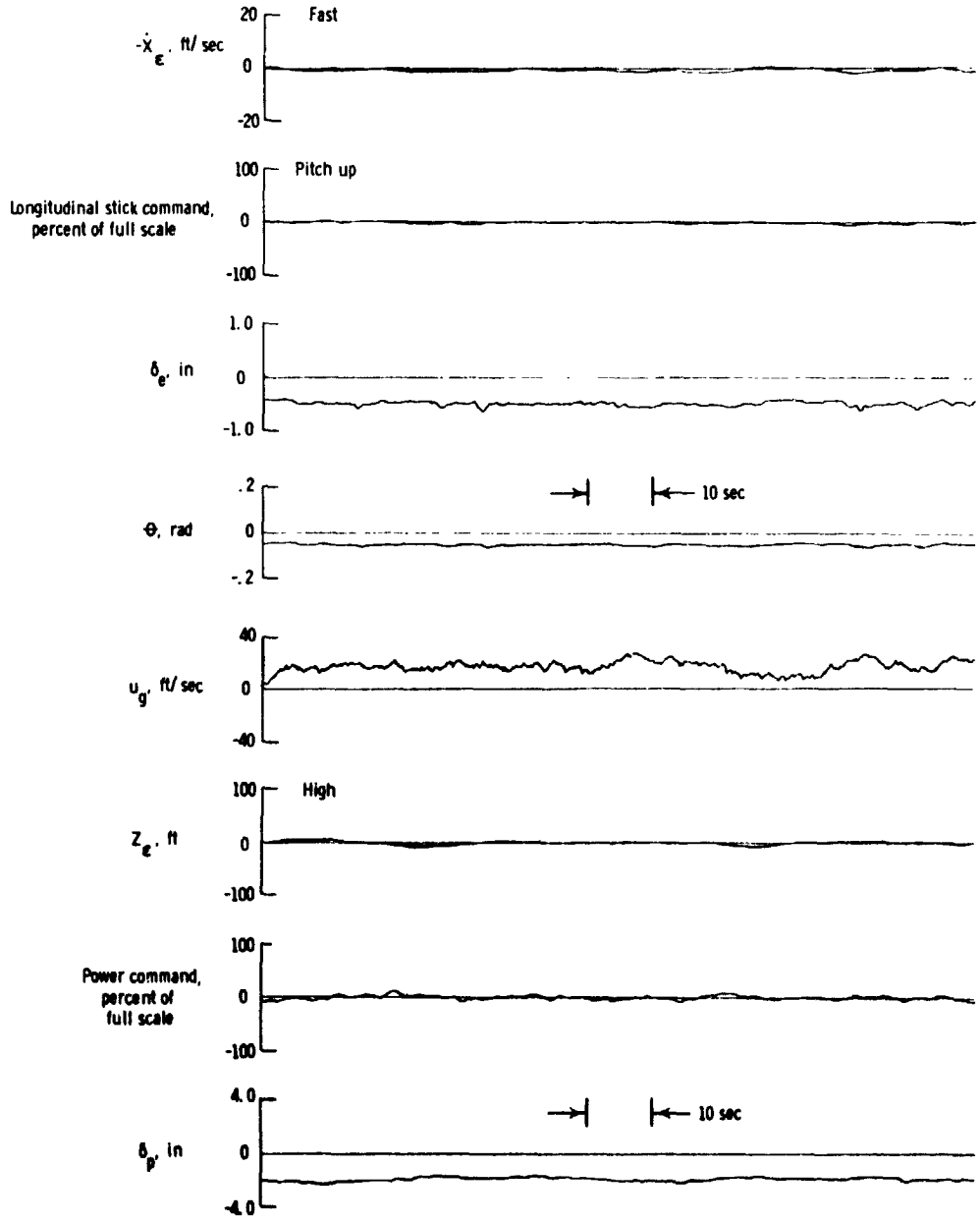

Figure 35.- Time histories for a 45-knot, 6-degree glide slope approach (turn following).

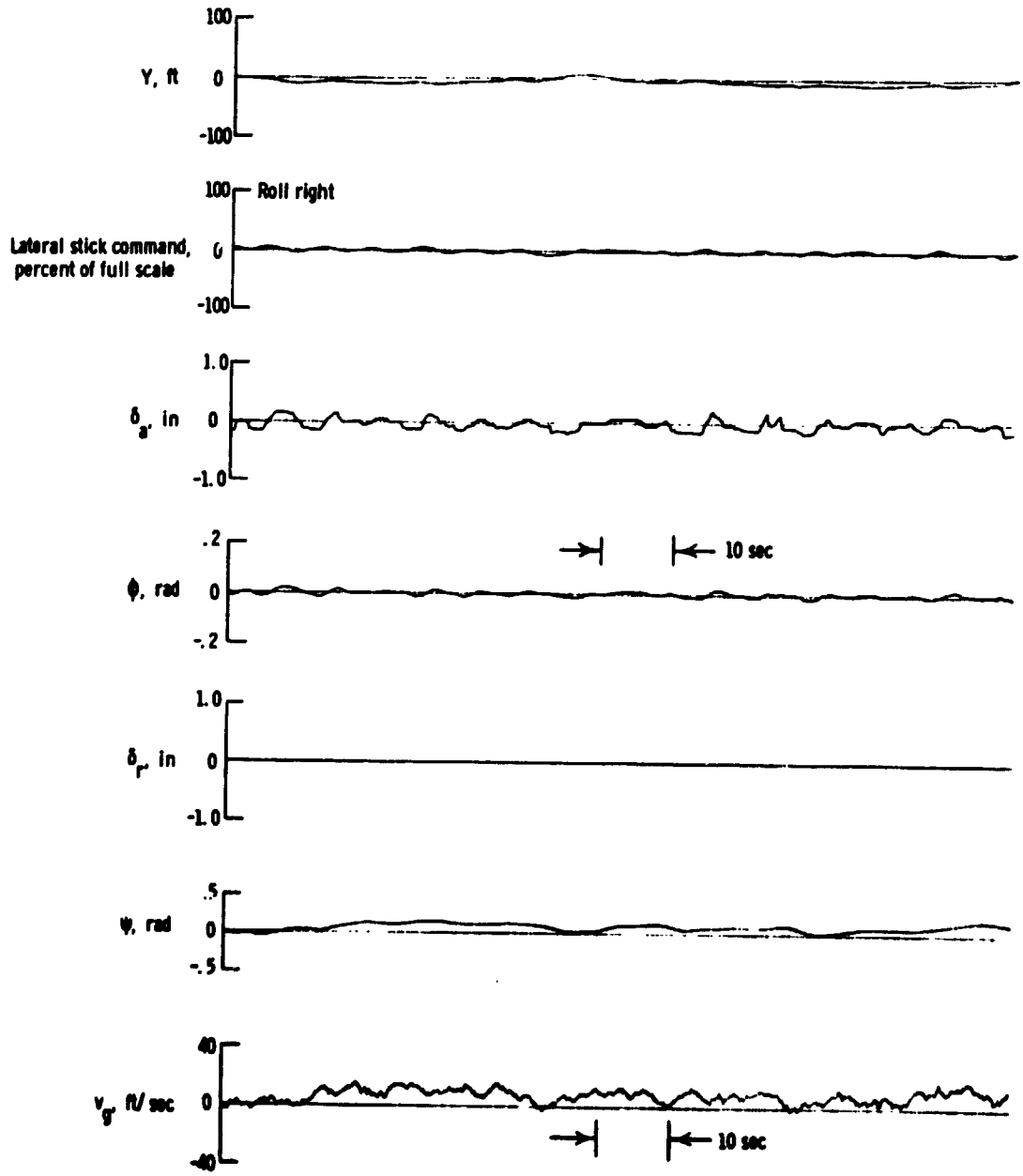

(b) Lateral control axis.

Figure 35.- Concluded.

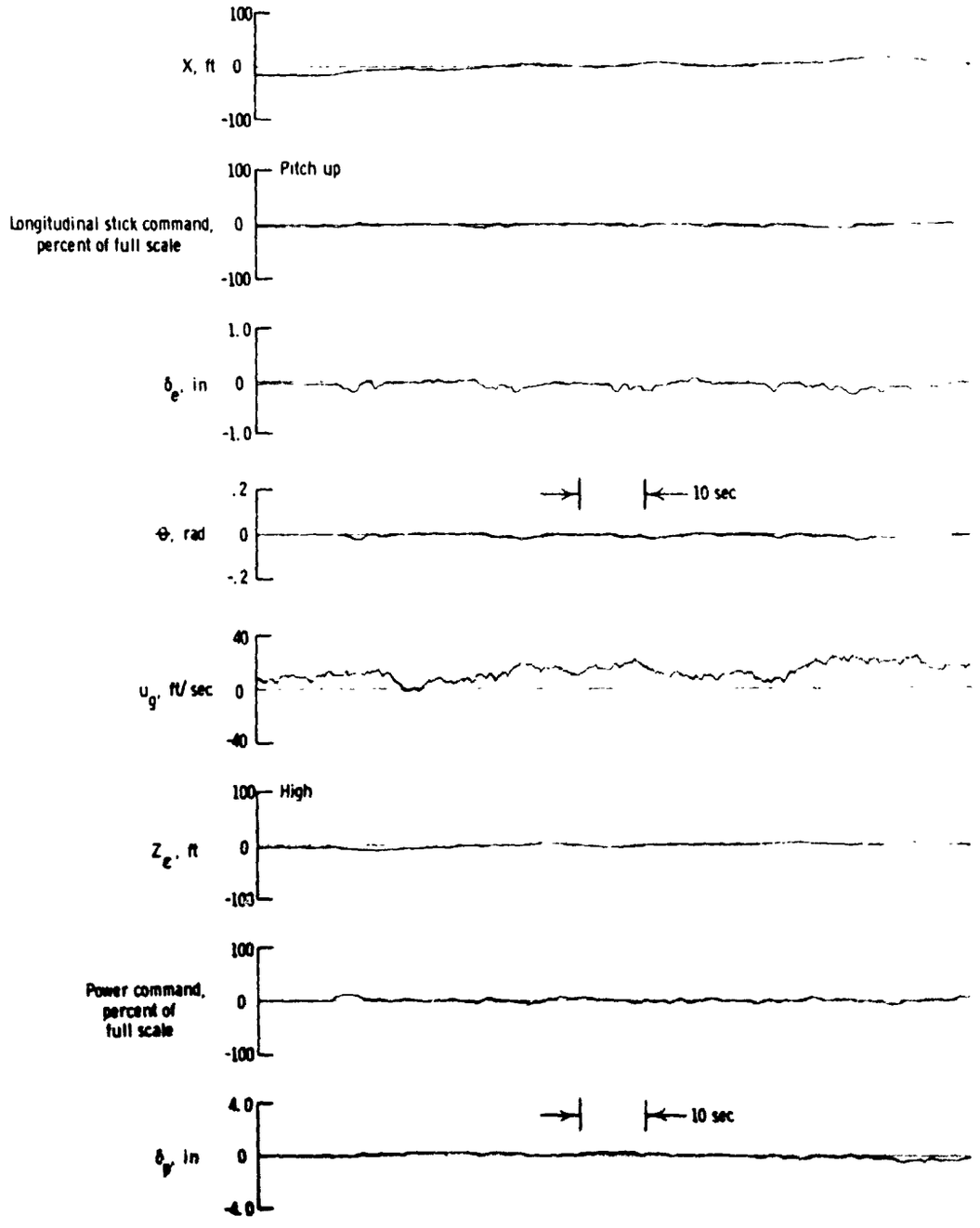

Figure 36.- Time histories for instrument hovering (heading hold).

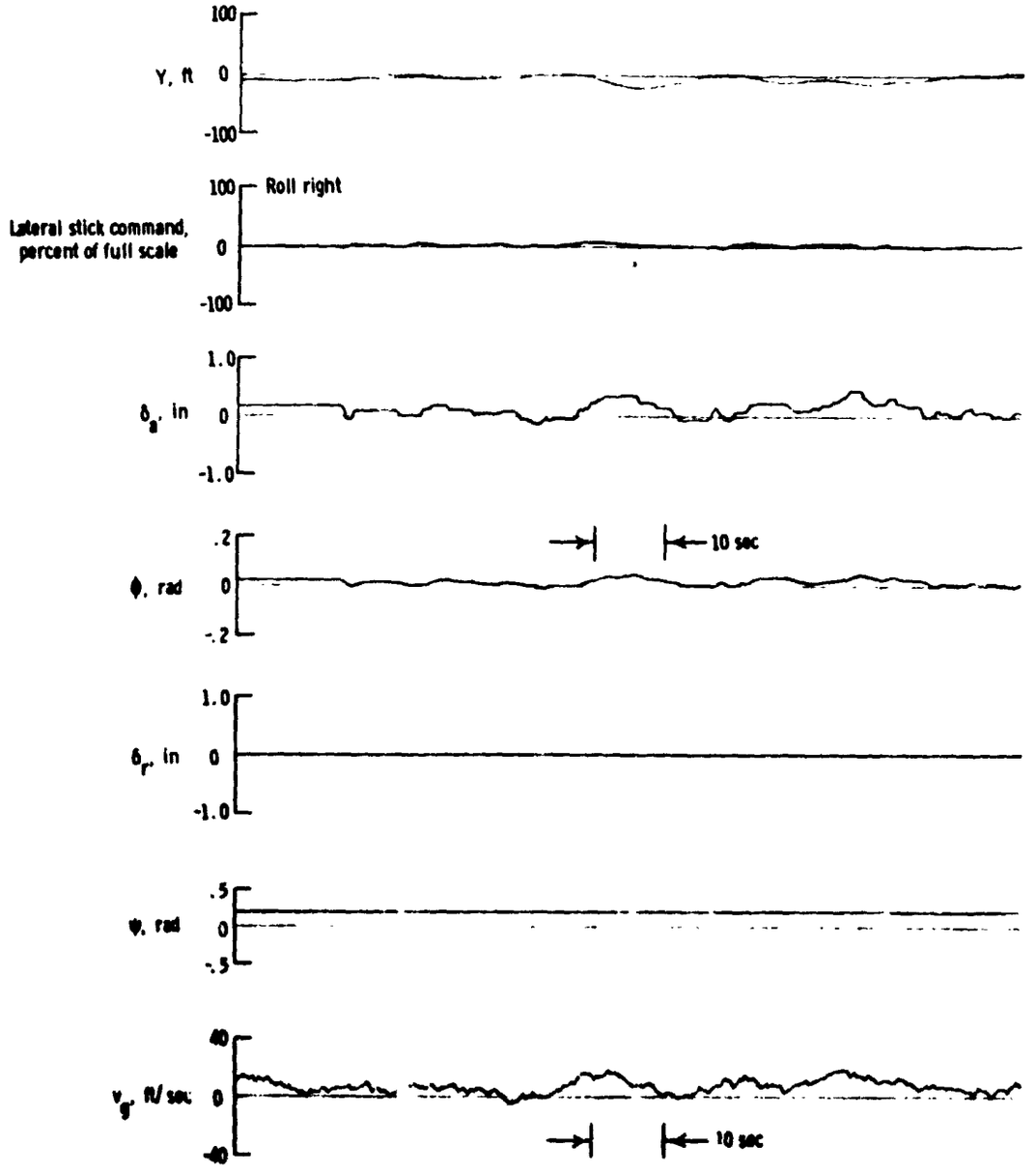

(b) Lateral control axis.

Figure 36.- Concluded.

CHAPTER V

CONCLUDING REMARKS

A control theory analysis of a three-axis flight-director for a specific VTOL configuration has been made, and in addition, a fixed-base simulator evaluation of the flight-director commands has been conducted. On the basis of this study, it appears highly advantageous to use conventional control theory methods in the design of flight-director systems, thereby minimizing the dependence on inefficient trial-and-error techniques. The analytical approach provides an intricate understanding of the sensitivity of the overall system to the various parameters and results in a more nearly optimized flight director.

Some generalized results with regard to such an analytical approach have been obtained. To effect a flight-director command which can be controlled by the pilot with a minimum of effort, it appears desirable to include an inner-loop flight-director term which approximates a first-order lag in response to the pilot's control input. Furthermore, it is neither necessary nor desirable to use sensitive zero-order feedback terms, such as the control position signal itself. By assuming an appropriate pilot model based on these inner-loop dynamics, it is possible to adjust the flight-director gains of the outer-loop terms in a manner similar to that for an automatic control system in order to achieve the desired outer-loop response.

BIBLIOGRAPHY

BIBLIOGRAPHY

1. Adams, James J.; and Bergeron, Hugh P.: "Measured Variation in the Transfer Function of a Human Pilot in Single-Axis Tasks." Washington, D. C.: National Aeronautics and Space Administration, 1963. (NASA TN D-1952.)

2. Blakelock, John H.: Automatic Control of Aircraft and Missiles. New York: John Wiley and Sons, Inc., 1965.

3. Boeing-Vertol Division: "Tandem Helicopter Trim and Stability Analysis." Morton, Pennsylvania: Boeing Vertol Division, March 25, 1965. (Aerodynamics Investigation III-264.)

4. Brotherhood, P.: "An Investigation of the Guidance and Control of the Helicopter Using Flight Directors in Beam Approaches at Angles up to 30°." London: Ministry of Aviation, May 1961. (Tech. Note No. Naval 46, British Royal Aircraft Establishment.)

5. Dorf, Richard C.: Modern Control Systems. Reading, Massachusetts: Addison-Wesley Publishing Co , 1967.

6. Garren, John F., Jr., et al.: "Flight Investigation of VTOL Control and Display Concept for Performing Decelerating Approaches to an Instrument Hover." Washington, D. C.: National Aeronautics and Space Administration, 1971. (NASA TN D-5860.)

7. Kelley, Charles R.: Manual and Automatic Control. New York: John Wiley and Sons, Inc., 1968.

8. Kelly, James R.; Niessen, Frank R.; and Sommer, Robert W.: "Evaluation of a VTOL Flight-Director Concept During Constant-Speed Instrument Approaches." Washington, D. C.: National Aeronautics and Space Administration, 1970. (NASA TN D-5860.)

9. McRuer, Duane T ; and Jex, Henry R.: "A Review of Quasi-Linear Pilot Models," Institute of Electrical and Electronics Engineers Transactions, Vol. HFE-8, No. 3, September 1967, pp. 231-249.

10. McRuer, Duane T.; and Klein, R. H.: "A Pilot-Vehicle Systems Approach to Longitudinal Flight Director Design." New York: American Institute of Aeronautics and Astronautics, August 1970. (Preprint 70-1001.)

11. Scott, Charles M., Jr.: "V/STOL Flight Director Systems." New York: American Helicopter Society, November 1970. (Preprint SW-70-28.)

12. Tapscott, Robert J., et al: "VTOL Instrument Flight Research Relating to Aircraft Requirements and Operating Characteristics for the Terminal Area." New York: American Institute of Aeronautics and Astronautics, October 1970. (Preprint 70-1333.)